Title: Tissue engineered organoid co-culture model of the cycling human endometrium in a fully-defined synthetic extracellular matrix**.**

Authors: Juan S. Gnecco[1,2,#], Alexander Brown[1,2,#], Kira Buttrey[2], Clara Ives[1,2], Britt Goods[3], Lauren Baugh[1,2], Victor Hernandez-Gordillo[1], Megan Loring[1,3], Keith Issacson[1,3], and Linda G. Griffith*[1,2]

Affiliations: *[1]Center for Gynepathology Research, [2]Department of Biological Engineering, Massachusetts Institute of Technology, 77 Massachusetts Ave, Cambridge MA, USA 02139. [3]Newton Wellesley Hospital, Newton, MA USA 02115. [3]Thayer School of Engineering at Dartmouth College, Hanover, NH.*

 # Equal contribution

*** Corresponding author:** L.G.G. (griff@mit.edu)
Massachusetts Institute of Technology
Room 16-429
77 Massachusetts Ave
Cambridge, MA 02139
ph (617)253-0013

Abstract:

The human endometrium is a mucosal barrier that undergoes cycles of growth, differentiation, and breakdown in response to sex hormone fluctuations. Dynamic tissue responses to hormones are primarily driven by epithelial-stromal communication and its dysregulation is linked to myriad gynecological disorders. The lack of robust *in vitro* models for the long-term 3D co-culture of patient-derived endometrial epithelial and stromal cells hinders dissection of this crosstalk and thus impairs progress in disease treatment. Here, we describe a versatile synthetic extracellular matrix tailored to the endometrium that enables the *in vitro* modeling of human healthy and disease states across the menstrual cycle. We used a tissue-inspired approach to semi-empirically screen a parameter space that encompasses the biophysical and molecular features of the endometrial microenvironment. Leveraging cell-specific integrin expression profiles, we defined a modular polyethylene glycol (PEG)-based hydrogel that fosters hormone-driven expansion and differentiation of epithelial organoids co-cultured with stromal cells. Characteristic morphological and molecular responses of each cell type to hormone changes were observed when cells were co-encapsulated in hydrogels tuned to a stiffness regime similar to the native tissue and functionalized with a collagen-derived adhesion peptide (GFOGER) and a fibronectin-derived peptide (PHSRN-K-RGD). Using transcriptomic and functional assays, we demonstrate the system's ability to recapitulate menstrual-cycle specific reproductive events and identified that inflammation-induced dysregulation of epithelial proliferation is mediated via the stromal compartment. Altogether, we demonstrate the development of a fully synthetic matrix to sustain the dynamic changes of the endometrial microenvironment and support its applications to understand endometriotic diseases.

1. Introduction:

The endometrium is the mucosal lining of the uterus in which the establishment and maintenance of pregnancy occurs[1]. It is a highly dynamic tissue that undergoes spatial and temporal changes in response to endocrine signaling by the ovarian sex hormones estradiol (E_2) and progesterone (P4). Cyclical changes in these hormones dictate the timing and functional capabilities of the endometrium to support nidation by driving cell-specific morphological and biochemical processes[2]. Histologically, the endometrium is primarily composed of the hormone-responsive epithelium and specialized reticular fibroblasts (stromal cells) embedded in a dynamic extracellular matrix (ECM).[3–5] Endocrine-mediated reproductive function is mediated through both direct and indirect mechanisms governed by the crosstalk between these cell populations.[6–8] The idealized 28-day human menstrual cycle is characterized by three distinct phases in which the endometrium undergoes E_2-mediated tissue regeneration (the 'proliferative phase') followed by a 14-day P4-dominant phase (the 'secretory phase') that governs the differentiation processes necessary for the successful establishment of pregnancy (Fig 1A). In the absence of embryo implantation, a sharp withdrawal of hormones triggers a cascade of inflammatory processes that results in a rapid influx of leukocytes and cellular apoptosis that promote the shedding of the endometrial tissue (the 'menstrual phase') after which the cycle initiates again.[3,4] Despite the fundamental role E_2 and P4 play in maintaining reproductive and systemic functions, a thorough understanding of the cellular mechanisms driving these processes remains elusive due in part to a lack of physiological models that recapitulate the complex multi-cellular human condition.[3,9]

Experimental models capable of recapitulating epithelial-stromal crosstalk are necessary to understand human reproductive physiology and pathology. Endometrial stromal cells (ESCs) are historically the most utilized primary cell type for experimentation in reproductive biology due to their ability to be cultured and expanded *in vitro*. However, the isolation, culture, and expansion of primary endometrial epithelial cells has been a challenge. Recently, protocols to harvest, expand, and maintain primary endometrial epithelial cells as endometrial epithelial organoids (EEOs) have been developed. Organoids are self-organizing 3D cell structures that retain many physiologically relevant and functional features of their native tissues of origin.[10] thus, EEOs provide opportunities to investigate human reproductive function, understand disease pathogenesis[11], and test therapeutic compounds for clinical applications.[12,13] EEOs can be generated from isolated primary adult endometrial glands embedded in Matrigel, a complex, tumor-derived ECM primarily composed of heterogenous basement membrane (BM) proteins and growth factors (GFs), and a defined culture medium designed to enrich the expansion of the

78 stem/progenitor compartment.[14,15] Clonally-generated EEOs retain columnar epithelial
79 architecture of the native tissue and form polarized cyst-like structures that are genomic stable,
80 hormone-responsive, and cell-heterogenous.[12,13,16] However, the reliance on Matrigel to
81 establish organoid systems presents a critical obstacle for numerous experimental, analytical,
82 and therapeutic applications for dynamic and hormone-sensitive tissues such as the
83 endometrium.[17,18] Matrigel's inherent lot-to-lot variability, poorly-defined molecular composition,
84 and limited tunability in biophysical and biomolecular properties have driven efforts to develop
85 synthetic (or semi-synthetic) ECMs that are fully defined, modular, and tunable.[11,19–27]
86 Although models that introduce the epithelial and stromal compartment in 3D using
87 naturally-derived hydrogels have been developed, they are severely limited by a rapid ECM
88 consumption and loss of ECM integrity, which ultimately leads to highly abbreviated and artificial
89 experimental conditions.[28–31] Moreover, these models often lack the biophysical and molecular
90 composition of the native endometrium that can reliably support the morphogenic and
91 simultaneous functional behavior of multiple cell types. Recently, the development of fully or
92 semi-synthetic ECMs to culture enteric organoids were reported for both; murine[24,32] and
93 human[18,22,27,32] tissues. We have previously demonstrated using cell lines that poly(ethylene
94 glycol) (PEG)-based hydrogel systems can be applied to model the endometrial mucosal
95 barrier.[26] We recently identified a completely synthetic hydrogel formulation designed for the
96 culture, differentiation and passaging of human intestinal enteroids that also supported other
97 epithelial-derived tissues, including endometrial epithelial cells[27]. Furthermore, we have recently
98 implemented this matrix to support the culture of pancreatic tumor organoids with a complex
99 stroma.[33] Despite these advances, a fully-defined synthetic ECM that can support the long-term
100 culture and function of multiple endometrial cell populations still predominates as an unmet
101 need.
102 Inspired by the integrin expression and ECM composition found in the native tissue, we
103 designed a hydrogel matrix that targets cell-specific integrins, supports cell-secreted ECM
104 deposition, and mimics the biophysical properties of the endometrium. Here, we developed a
105 bio-labile PEG-based synthetic ECM that supports the simultaneous culture of primary human
106 EEOs and ESCs in a 3D co-culture model of the endometrium that recapitulates the sex
107 hormone-induced phases of the human menstrual cycle. We validated the system using a 15-
108 day *in vitro* co-culture that robustly modeled the phases associated with a human menstrual
109 cycle. Moreover, we utilized this co-culture model to examine how inflammatory stimuli
110 promoted disease-associated progesterone resistance and morphological aberrations
111 suggestive of a dysfunctional endometrium. Altogether, this synthetic ECM supported the

112 generation of a multi-cellular tissue engineered endometrium that recapitulates key reproductive
113 physiological and pathological processes, representing a significant advance in our ability to
114 model and study human reproductive function and diseases *in vitro*.
115

116

117 **2. Methods:**

118

119 ***2.1. Tissue Acquisition and Isolation of Human Endometrial Cells***

120 All participants provided informed consent in accordance with a protocol approved by the
121 Partners Human Research Committee and the Massachusetts Institute of Technology
122 Committee on the Use of Humans as Experimental Subjects (Protocol number IRB-P001994).
123 Endometrial tissue was obtained from pipelle biopsies from reproductive age women (N=18,
124 ages 18-45, Fig S15) undergoing laparoscopic surgery for non-malignant gynecologic
125 indications. Study enrollment was limited to pre-menopausal women and excluded patients with
126 an irregular or ambiguous cycle or a history of hormone use in the 3 months prior to
127 surgery. Endometrial epithelial glands and stromal cells were isolated by enzymatic digestion
128 and filter-separated as previously described[34] resulting in ≥ 95% purity as assessed by positive
129 staining for vimentin and morphological assessment. Briefly, single stromal cells were separated
130 from intact epithelial glands fragments and cultured separately. Stromal cells were expanded in
131 traditional 2D cultures (as described below) and epithelial glands were cultured as organoids
132 using protocols adapted from Turco et al.[35] All cells were passaged a maximum of 5 times for all
133 experimental *in vitro* assessments.

134

135 ***2.2. Cell Isolation and Endometrial Organoid Generation***

136 Stromal cells were maintained in phenol red-free DMEM/F12 with 5% charcoal-stripped calf
137 serum, 1 nM 17-β estradiol (E_2, Sigma Aldrich) and 1× Pen-Strep solution (Sigma Aldrich).
138 Some cell cultures were treated with 500 nM synthetic progesterone medroxyprogesterone
139 acetate (MPA, Sigma Aldrich). Primary endometrial epithelial organoids (EEOs) were generated
140 from the primary epithelial fragments (p0) according to established protocols and maintained in
141 endometrial epithelial organoid expansion medium (EEO medium).[12,13] EEO media is modified
142 from elsewhere.[36] Briefly, EEO media was composed of advanced basal media (1X); rhEGF (50
143 ng/mL, Corning); rhNoggin (100 ng/mL, Peprotech); rhRspondin-1 (200 ng/mL, R&D systems);
144 rhFGF-10 (50 ng/mL, Peprotech); Estradiol (E_2, 1nM, Sigma Aldrich); Nicotinamide (1mM);
145 Insulin-Transferrin-Selenium (ITS, 1%, Invitrogen); N-Acetyl-L-Cysteine (1.25 mM); TGFB
146 pathway inhibitor (A83-01, 500 nM, Peprotech); and Rock inhibitor Y-27632, (ROCKi, 10 μM,
147 Tocris) which was utilized for the initial culture set up and for 4 days post seeding. For seeding,
148 epithelial cells, as fragments or single cell suspensions, were embedded in 70% Matrigel and
149 cultured for 6 days, media was changed every two days (Fig S2). For passaging, 6-day old

150 organoids were incubated in Cell Recovery Solution (CRS, Gibco) for 30 mins at 4°C to dissolve
151 Matrigel, then pelleted and digested with Tryp-LE supplemented with 1:100 DNAse (40k units,
152 Sigma) for 15 minutes in a 37°C water bath followed by mechanical dissolution to generate
153 single cells. For expansion, single epithelial cells were seeded in Matrigel at a density of 1,000
154 cells/µL in 60µL droplets in non-tissue culture treated plates. To establish co-cultures of ESC
155 and EEOs, ROCKi was omitted from EEO media. All media changes for the co-cultures
156 occurred every 3 days for up to 15 days unless noted otherwise. Spent conditioned media from
157 these cultures was collected and stored at -20°C for downstream analysis.
158

159 ***2.3. PEG hydrogel materials and peptides.***

160 8-arm poly(ethylene glycol) (PEG) macromers (20 kDa) functionalized with vinyl sulfone (20 kDa
161 PEG-VS) were purchased from JenKem Technology. All peptides were custom synthesized and
162 purified (>95%) by Boston Open Labs (Cambridge, MA), GenScript (Piscataway, NJ), or CPC
163 Scientific (Sunnyvale, CA). Peptides used in these studies include; a dithiol crosslinking peptide
164 containing a matrix metalloproteinase (MMP)-sensitive substrate (Ac)GCRD-LPRTG-
165 GPQGIWGQ-DRCG(Am) (***CL-LW***); a fibronectin (FN)-derived peptide containing both the
166 canonical RGD motif from the 10th FN type III domain as well as the PHSRN synergy site from
167 the 9th FN Type III repeat in a branched configuration akin to the biophysical presentation in FN,
168 (Ac)PHSRNGGGK-GGGERCG(Ac) -GGRGDSPY(Am) (***PHSRN-K-RGD***);[37–39] a Collagen I-
169 derived peptide, (Ac)GGYGGGPG(GPP)$_5$GFOGER(GPP)$_5$GPC(Am) (***GFOGER***);[22,40] a peptide
170 with affinity for sequestering cell-produced FN, (Ac)KKGCRE-TLQPVYEYMVGV(Am) (***FN-***
171 ***binder***);[41] and a peptide with affinity for sequestering the basement membrane proteins type IV
172 collagen and laminin, (Ac)GCRE-ISAFLGIPFAEPPMGPRRFLPPEPKKP(Am) (***BM-binder***).[42] All
173 peptides were reconstituted in acidic (pH 5.5) Milli-Q water (Millipore). The concentration of free
174 thiols in all peptides was determined using Ellman's reagent (Sigma Aldrich).
175

176 ***2.4. Fabrication of synthetic PEG extracellular matrix.***

177 All synthetic matrices were assembled to screen a range between 3-7 wt% PEG (w/v) using an
178 8-arm 20kDa PEG-VS backbone. Functionalization of the PEG-VS macromers (fPEG-VS) was
179 performed stepwise via Michael-type addition reaction according to the concentrations
180 determined prior to experimental set up. First, the PEG-VS macromer was diluted with 10X
181 PBS-HEPES solution (1 M, pH 8.2) at 10% total solution volume and ultrapure H_2O. Second, the
182 integrin binder peptides (***PHSRN-K-RGD***, ***GFOGER***) and the matrix-binder peptides (**FN-**
183 **binder, BM-binder**) were added to the reaction mixture, immediately vortexed and allowed to

184 react for 30 min at RT with at pH 7.8. Third, cells were counted, pelleted and gently
185 resuspended with functionalized PEG-VS (fPEG-VS). Finally, upon cell resuspension, the
186 crosslinker (CL-LW) was added to the mixture to initiate the gelation process, gently vortexed,
187 and plated accordingly, typically in 3 µL droplets in non-tissue culture treated 96-well plates
188 unless otherwise specified. Cell-fPEG-VS mixture was incubated for at least 25 minutes in a
189 humidified incubator at 37°C until hydrogels dollops were solidified. A test gel droplet was
190 utilized as a marker for complete gelation before the addition of media.
191

192 ### *2.5. Rheological characterization of hydrogels*

193 To measure bulk bio-mechanical properties of crosslinked gels, 25 µL of each gel matrix mixture
194 was loaded into a 1 mL syringe that had the tip cut off at the 0.1 mL mark. The matrix was
195 allowed to gel at 37 ºC for 25 min and then extruded from the open syringe as a cylindrical disc
196 and moved to a 24 well plate that contained 400 µL of 1X PBS. The plate was incubated for 24
197 hours in a humidified incubator at 37 ºC, 95% air, and 5% CO_2, to allow equilibrium swelling to
198 occur prior to rheological characterization. This procedure generates hydrogel discs of 1.4 mm
199 in thickness. The discs were sandwiched between an 8 mm sandblasted parallel plate geometry
200 and sandblasted base. The shear modulus was determined by performing small-strain
201 oscillatory shear measurements on an Anton Parr MCR 302 rheometer. The mechanical
202 response was recorded by performing frequency sweep measurements (0.1–10 Hz) at a
203 constant strain (0.05), at 37 °C. The elastic modulus (E) is reported as a measure of bulk matrix
204 mechanical properties derived from the recorded storage modulus (G') in the linear elastic
205 regime where: $E = 2G'(1 + \nu)$ with the assumption that ν = 0.5 for ideal elastic hydrogel
206 materials.
207

208 ### *2.6. EEO generation in synthetic hydrogels*

209 Endometrial organoids were established and expanded in Matrigel according to established
210 protocols[12] with some minor modifications. Lumenized organoids with a diameter greater than
211 100 µm were harvested with cold Cell Recovery Solution (CRS, ThermoFisher). Matrigel dollops
212 were manually detached with a wide bore pipette tip, making sure to fully scrape the entire well
213 to lift off the entire gel. The dollops were resuspended in cold CRS (5mL) for at least 30 mins on
214 ice to dissolve remaining Matrigel, followed by centrifugation at xxxxx, which resulted in a clear
215 pellet of organoids. Organoids were broken into single cell suspensions using 1mL of
216 prewarmed TypLE Express (ThermoFisher) supplemented with DNAase (10µl, 1:100) and
217 continuous mechanical agitation until a single cell suspension of epithelial cells was observed.

218 Single cells were counted using a hemocytometer then resuspended in the functionalized PEG
219 precursor (fPEG-VS) solutions prior to the addition of the crosslinker. In parallel, single cells
220 were resuspended in Matrigel that served as an experimental control during matrix evaluation.
221 In both cases, cells were encapsulated at a density of 500 cells/μL of matrix. Cell-matrix
222 suspensions were seeded as 3 μL droplets on a non-tissue treated 96 well plate and allowed to
223 polymerize for 25 min in a humidified incubator at 37 ºC, 95% air, and 5% CO_2. Complete
224 gelation was examined visually on a test gel droplet prior to the addition of media. Gel droplets
225 were maintained in 100 μL of expansion EEO media supplemented with Y-27632 (10 μM).
226 Media was changed every three days.
227
228 ***2.7. Generation of co-culture model***
229 Six-day old intact organoids (~100 μm diameter) were grown and expanded in Matrigel and
230 harvested as described above. To maintain EEO integrity, organoids were incubated in Cell
231 Recovery Solution until Matrigel was fully dissolved. Careful resuspension of intact EEOs in
232 DMEM/F12 was performed to prevent disrupting EEO integrity. In parallel, donor matched ESCs
233 were expanded using traditional 2D polystyrene cell culture plates and grown to 80%
234 confluency. ESCs were lifted from 2D culture plates using trypsin (1X) and processed to
235 generate a single cell suspension. Intact EEOs and ESCs were prepared in parallel to
236 encapsulate both cell types simultaneously and establish a co-culture in the PEG matrix
237 solution. Cells were encapsulated at a density of 10,000 ESC and 10 intact EEOs per μL of
238 matrix. This epithelial-stromal ratio was determined experimentally based on the cell ratios
239 utilized to generate established endometrial xenograft models (sub-renal capsule) described
240 elsewhere[43,44] and validated using whole-mount 3D image analysis of endometrial tissue we
241 performed (Fig S5). Embedded cells in fPEG-vs were seeded in 3 μL droplets and allowed to
242 polymerize as described above in non-tissue culture treated 96-well plates. Co-culture was
243 maintained in EEO media without Y-27632. Media was changed every three days and
244 maintained for up to 15 days. It was noted that some basal components of the organoid medium
245 contained P4 (N2 and B27) which may impact hormone responsive behavior, so a 'neutral'
246 formulation of this organoid medium (nEEO medium) that completely lacked P4 was tested in
247 some co-cultures. Matching monocultures of ESCs-only or EEOs-only were established in
248 parallel for some experiments. Cultures were imaged daily.
249
250 ***2.8. EEO and co-culture efficiency and quantification***

251 To quantify organoid diameter and total organoid formation efficiency, single epithelial cells
252 were encapsulated in fPEG-VS hydrogels or Matrigel and cultured over 14 days. EEO formation
253 efficiency was calculated as the percentage of organoids with a clear lumen with a diameter
254 (>100 um) relative to Matrigel. 4X brightfield (BF) z-stack images of 10-day old endometrial
255 organoids were captured using an EVOS M500 microscope (Invitrogen). The images were
256 processed in Fiji using the time lapse Gaussian-based stacker focuser plugin to generate
257 maximum intensity projections. Images were analyzed a deep learning based algorithm as
258 described previously to produce a diameter distribution for each condition[45]. Daily images of co-
259 culture were manually curated to obtain relative growth rates of the organoids in single culture
260 or co-culture by measuring EEO diameter and quantifying the daily fold change relative to day 1
261 of culture (video 4,5).
262

263 ***2.9. RNA isolation for quantitative real time PCR (qPCR) and bulk RNA-seq.***

264 ESCs and intact EEOs cultured in Matrigel or synthetic hydrogels were used for molecular
265 analysis. After 14 days of culture, intact EEOs were released from Matrigel and the synthetic
266 ECM, using Cell Recovery Solution, or recombinant Sortase, respectively. Intact EEO-only
267 cultures, ESC-only cultures, or Co-cultures were pelleted, resuspended in TRIzol reagent
268 (ThermoFisher Scientific), and then stored at -80°C until processing. RNA was extracted using
269 the Directzol RNA Mini-Prep kit (Zymo Research) per the manufacturer's protocols with the
270 inclusion of an on-column DNase step using the PureLink DNase Set (ThermoFisher Scientific).
271 At least eight replicates (3 µl droplets) were pooled together to obtain sufficient RNA. cDNA was
272 synthesized from ~1 µg of total RNA using the High-Capacity RNA-to-cDNA Kit (ThermoFisher
273 Scientific, 4387406) per manufacturer's protocols. TaqMan Fast Advanced Master Mix
274 (ThermoFisher Scientific) was used in congruence with the cell-specific probes for qPCR. Gene
275 expression was determined using the StepOnePlus real-time PCR system (Applied Biosystems)
276 and calculated using the ΔΔCt method using GraphPad Prism. Gene expression was first
277 normalized using the housekeeping GAPDH gene in each sample, then the relative fold change
278 relative to experimental control. High Throughput 3' Digital Gene Expression (3'DGE) RNAseq
279 was performed on the isolated RNA using NovaSeq flowcells at the BioMicroCenter (MIT) and
280 processed using the BMC/BCC 1.8 pipeline.
281

282 ***2.10. Secreted protein measurement by ELISA and Luminex***

283 Spent media was stored at −80°C until analyzed by ELISA for prolactin (R&D systems).
284 Protocols provided by the manufacturer were adapted to allow ELISAs to be performed in a

285 384-well plate (ThermoFisher) to minimize medium (sample) volume needed.[26] Multiplexed
286 Luminex assays were performed to measure cytokines in 48- or 72-hour undiluted conditioned
287 medium throughout the co-culture period using the magnetic Human Luminex XL Cytokine 45-
288 PLEX pre-mixed kit (R&D systems). Protocols provided by the manufacturer were adapted to
289 allow the assay to be performed in a 384 well plate to avoid introducing batch variability. Ten-
290 point standard curves with culture medium and assay buffer blanks were included for
291 quantification. Conversion from mean fluorescence intensity (MFI) values to absolute
292 concentration was performed by interpolating 5-parameter logistical fits of standard curves for
293 each analyte. Following the same downstream analysis protocol, secreted matrix
294 metalloproteinases (MMP) concentrations were measured using the magnetic Human MMP
295 Magnetic Luminex Performance Assay (R&D Systems). This assay required dilutions of cell
296 culture supernatants in fresh culture medium at either 2x or 200x in order to detect the reported
297 analytes within a quantifiable range.
298
299 ***2.11. Immunostaining and image analysis***
300 Hydrogel samples were fixed in 4% paraformaldehyde (Electron Microscopy Sciences) for 30
301 mins, permeabilized in 0.2% TritonX-100 in PBS (Sigma) for at least 30 mins at room
302 temperature, and then blocked overnight with blocking buffer (1% BSA (Sigma), 5% normal
303 donkey serum (Electron Microscopy Sciences) in PBS) at 4°C. Hydrogels were incubated with
304 primary antibodies overnight while rocking at 4°C, rinsed with blocking buffer 3 times (5 min
305 each while rocking at RT), and treated with secondary-conjugated antibodies overnight while
306 rocking at 4°C. Specific antibodies can be found in the supplementary table of reagents. Images
307 were captured using a ZEISS confocal Laser Scanning Microscope (LSM 880) or a Keyence
308 BZ-X800 Fluorescence Microscope. Image analysis was performed using Fiji open software and
309 3D image processing was performed using Imaris (Bitmap) software (9.6.0).
310
311 ***2.12. Endometrial ECM proteomics***
312 Endometrial ECM processing for proteomics, proteomics data collection, processing and
313 analysis is described elsewhere (in preparation). Briefly, fresh endometrial biopsies were
314 collected and processed using 50 µl of RapiGest (Waters Corporation) reconstituted in 50 mM
315 NH_4HCO_3 at a concentration of 2mg/ml to digest the endometrial biopsy sample for 24 hours at
316 37˚C. Next, urea (ThermoFisher) and dithiothreitol (ThermoFisher) were added to the sample to
317 bring the mixture of a final concentration of 4 mM and 5 mM, respectively. Finally,
318 iodoacetamide (MilliporeSigma) was added to the sample, for a final concentration of 15 mM

319 and kept in the dark, at 37˚C, for 30 minutes. Samples were frozen at -80˚C until all patient
320 samples had been collected and processed. Samples were lyophilized overnight and then
321 reconstituted in NH_4HCO_3. Samples were digested with Trypsin Gold, mass spectrometry grade
322 (Promega), using a ratio of 1 µg trypsin to 50 µg sample protein as quantified using a Pierce
323 BCA Protein Assay Kit (ThermoFisher). Samples were digested overnight at room temperature
324 using a rotor for mixing and then placed in a speed vacuum to reduce sample volume. Dried
325 down digested peptide samples were labeled with TMT10plex kit (Pierce). After labeling, the
326 samples were mixed and purified with peptide desalting spin columns (Pierce). 1/5 of the
327 sample was used for one LC/MS/MS analysis (Thermo Exploris480 mass spectrometer). The
328 dried peptide mix was reconstituted in a solution of 2% formic acid (FA) for MS analysis.
329 Peptides were loaded with the autosampler directly onto a 50cm EASY-Spray C18 column
330 (Thermo Scientific). All MS/MS samples were analyzed using Sequest (Thermo Fisher
331 Scientific; version IseNode in Proteome Discoverer 2.3.0.523). Sequest was set up to search
332 uniprot_human_reviewed_032120.fasta (version March 21, 2020) assuming the digestion
333 enzyme trypsin. Scaffold Q+ (version Scaffold_5.0.1, Proteome Software Inc.) was used to
334 quantitate Label Based Quantitation peptide and protein identifications. Peptide identifications
335 were accepted if they could be established at greater than 10.0% probability to achieve an FDR
336 less than 1.0% by the Percolator posterior error probability calculation.[46] Normalization was
337 performed iteratively (across samples and spectra) on intensities, as described in Statistical
338 Analysis of Relative Labeled Mass Spectrometry Data from Complex Samples Using ANOVA.[47]
339 Medians were used for averaging. The protein list was then compared to the curated human
340 matrisome (http://matrisome.org/) list to look for ECM proteins. Samples were normalized using
341 a mixed aliquot of all patient samples that was analyzed in each LC/MS-MS run. Overlapping
342 ECM proteins found in all 3 LC/MS-MS runs were identified and the Limma package[48] in R was
343 used to remove batch to batch effects.
344

345 ***2.13. Endometrial tissue single cell RNA sequencing (scRNAseq)***

346 scRNAseq data collection, processing and analysis as described elsewhere (in preparation).
347 Seq-Well was performed as described previously[49,50]. Briefly, at least 15,000 cells were loaded
348 onto each array preloaded with barcoded mRNA capture beads (ChemGenes). Arrays were
349 washed with protein-free RPMI media, then sealed with plasma-treated polycarbonate
350 membranes. Reverse transcription was performed with Maxima H Minus Reverse Transcriptase
351 (ThermoFisher), excess primers were removed using an Exonuclease I digestion (New England
352 Biolabs), and whole transcriptome amplification (WTA) by PCR was performed using KAPA Hifi

353 PCR Mastermix (Kapa Biosystems). WTA product was purified using Agencourt Ampure beads
354 (Beckman Coulter) and 3' digital gene expression (DGE) sequencing libraries were prepared
355 using Nextera XT (Illumina). Arrays were sequenced using custom primers on a Novaseq S4.
356 All data were normalized, the top 2,000 variable genes identified. Initial clustering was
357 performed, and cell types were assigned on the basis of marker genes identified using Seurat's
358 Wilcoxon rank-sum test. All scripts to reproduce analyses are available for download
359 (https://github.com/bagoods).
360

361 ***2.14. Bulk RNAseq analysis of In Vitro co-cultures***

362 Aligned RNAseq transcript expected counts were analyzed in R (version 4.0.0) where data was
363 modeled using the edgeR package (version 3.34.0).[51,52] Counts were normalized by library size
364 and filtered to exclude genes with less than 20 transcripts across all samples. Principal
365 component analysis was performed using data batch-corrected by donor via the ComBat-seq
366 method of the sva package (version 3.13) in R, and each gene was scaled to have unit variance
367 before modeling.[53] Differential gene expression was calculated by modeling transcript data in a
368 quasi-likelihood negative binomial generalized log-linear model using the edgeR function
369 "glmQLFit". The use of a generalized log-linear model allowed for differences between hormone
370 treatment groups to be compared while accounting for inter-donor variability. Genes were
371 ranked by fold change in expression between hormone treatment groups to produce a ranked
372 list of genes for gene set enrichment analysis (GSEA)
373 (http://www.broadinstitute.org/gsea/index.jsp).Gene ontology (GO) term analysis was performed
374 on ranked gene lists of genes with pvalues <= 0.05. No adjustment was performed at this step
375 due to the low sample number, high variability, and intent to use the RNA sequencing as a
376 hypothesis generation step. The R package topGO (version 2.44.0) was used for GO term
377 identification and the package clusterProfiler (version 4.0.2) was used for visualizations. A
378 curated list of menstrual related genes was assembled from existing literature.[54,55] A heatmap of
379 $\log_2$ transformed data was created using the R package pheatmap (https://CRAN.R-
380 project.org/package=pheatmap; version 1.0.12) with the "complete" clustering method.
381

382 ***2.15. Statistical analysis***

383 Data are expressed as average ± standard error of the mean (SEM). Statistical analysis was
384 performed using GraphPad Prism 8. Unpaired t-tests assuming unequal variances and two-way
385 ANOVAs with appropriate post-tests were performed. Holm-Sidak's multiple comparison of the
386 mean or two-tailed Mann- Whitney tests when comparing two groups. qPCR data was analyzed

using multiple t-tests. Statistical significance was defined as * $p < 0.05$, ** $p < 0.01$, *** $p < 0.0001$, and ****$P < 0.0001$.

391 **3. Results**

392

393 ***3.1 Design of a fully synthetic ECM guided by multi-omic evaluation of human***
394 ***endometrium***

395 The ECM is an integral and dynamic component of the endometrial microenvironment that
396 mediates cellular and tissue-level function.[56] To engineer a fully synthetic ECM capable of
397 supporting physiologically relevant culture of endometrial cells *in vitro,* we leveraged a multi-
398 omic analysis of *ex vivo* human endometrial biopsies to characterize ECM composition and cell-
399 ECM interactions. Specifically, we utilized single cell RNA sequencing (scRNAseq, N=6), and
400 proteomic (LC-MS/MS, N=11) datasets from donors that represented the distinct phases across
401 the menstrual cycle.

402 Previous immunohistology studies have identified that integrin expression as being highly
403 dynamic across the human menstrual cycle[57]. However, the transcriptomic expression of
404 integrins of the endometrial microenvironment with single cell resolution has not been fully
405 evaluated. Here, we leveraged scRNAseq to characterize the integrin expression of endometrial
406 sub-populations within the cycling endometrium (Fig S1A-C) and identify the differentially
407 expressed integrins between "stromal" and "epithelial" compartments (Fig 1C). These cellular
408 compartments are known to modulate the functional changes in compositions of the ECM,[58–60]
409 therefore, we targeted these cell populations for the hydrogel design. Our analysis revealed that
410 across the menstrual cycle epithelial compartment primarily expressed the α1, α2, and α3
411 integrin subunits that are associated collagen binding, as well as the α6 subunit, which mediates
412 laminin (LMN) binding. ESCs primarily expressed the integrin α5 subunit, canonically involved in
413 fibronectin binding, throughout both the proliferative and secretory phase (Fig 1C). The RGD-
414 binding vitronectin receptor, integrin αV, was expressed by both cell populations and had a
415 dynamic expression profile in the epithelial compartment throughout the menstrual cycle,
416 corroborating previous findings that suggest it may play a specific role in embryo implantation.[57]
417 We validated these cell-specific integrin expression profiles *in vitro* using cultured ESCs and
418 epithelial cells (Fig S2D). Next, a proteomic analysis of the ECM composition was implemented
419 to characterize the matrisome of proliferative and secretory phase human endometrium.
420 Expression patterns largely varied according to cycle phase, suggestive of the ECM's dynamic
421 role in mediating key reproductive processes.[61–63] Specifically, most collagens and laminin
422 expression increased during the secretory phase while FN expression was higher in the
423 proliferative phase (Fig 1B).

424 Altogether, the identification of collagens, fibronectin, and laminin rich matrix and its
425 associated cellular integrin expression in endometrial cell populations of interest guided the
426 design of fully defined synthetic matrix. To accommodate the culture of epithelial and the
427 stromal compartment of the endometrium we targeted the engagement of the α2β1 and α5β1
428 integrins by utilizing synthetic peptide sequences that mimic the integrin binding sites of
429 collagen (*GFOGER, $\alpha 2\beta 1$*)[27,40] and fibronectin (*PHSRN-K-RGD, $\alpha 5\beta 1$*),[24,26] respectively. While
430 most other reports utilized a single peptide to maintain organoid[27] or stromal[26] cultures, we
431 hypothesized that a dual-peptide approach with both peptides would enable the establishment
432 of a co-culture platform. We functionalized an 8-arm poly(ethylene glycol) (PEG)-based
433 hydrogel with a combination of GFOGER and PHSRN-K-RGD (MIX). Moreover, to support the
434 dynamic hormone-induced nature of the endometrial laminin-based cell-ECM interactions,
435 matrix-binding peptides targeting cell-secreted FN and basement membrane (B.M.) proteins
436 (i.e., collagen IV/LMN) were also included in the matrix design (Fig 1D). We have previously
437 shown that incorporation of these peptides enhanced the accumulation of fibrillar collagen and
438 collagen IV/laminin-rich basement membrane deposition in cultures of endometrial cells.[26]
439 Finally, a protease-sensitive crosslinking peptide (*CL-LW*) was incorporated to enable cell-
440 mediated hydrogel remodeling during hormone-driven cellular morphogenesis and enable on-
441 demand bio-orthogonal matrix dissolution for cell release[26,38,64]. The tunable design of this
442 hydrogel system enabled the semi-empirical evaluation of matrix formulations to identify an
443 appropriate synthetic ECM that supports the culture and tissue-specific function of both
444 endometrial stromal and epithelial cell populations throughout the menstrual cycle (Fig 1D).
445
446 ***3.2 Synthetic ECM supports simultaneous culture of primary human endometrial stromal***
447 ***and epithelial cells***
448
449 *3.2.1. Establishment and characterization of EEO cultures in a synthetic hydrogel*
450 Protocols to establish and culture endometrial epithelial organoids (EEO) have transformed
451 our ability to study human endometrial epithelial cells *in vitro*[16]. Despite this, the reliance on
452 Matrigel as the gold-standard for EEO cultures limits experimental reproducibility and is not
453 conducive to maintain physiologically representative co-cultures with endometrial stromal cells.
454 To further characterize the biomolecular and biophysical properties on organoid establishment,
455 survival, and growth, EEO generation was evaluated across a range of relevant synthetic matrix
456 formulations (Fig 2A).

457 We previously showed a proof-of-principle that EEOs could emerge from single cells using a
458 relatively stiff synthetic matrix[27]. However, the characterization and hormone-induced
459 phenotypes of these organoids was relatively unexplored. Moreover, the influences of matrix
460 stiffness regimes that more closely mimic those of native endometrium were not investigated
461 systematically. These first-generation hydrogels were substantially stiffer (~2000 Pa), than the
462 native endometrial ECM (~250 Pa)[65] or Matrigel (~150-443 Pa)[21,66]. First, establishment of EEO
463 lines derived from single cells suspensions (scEEO) was demonstrated in synthetic matrices as
464 previously described (Fig 2A,E). The elastic modulus of synthetic gels was tuned by varying the
465 PEG polymer content from 3wt% (~300 Pa) to mimic native endometrial stiffness or to mimic a
466 pathologic state by increasing it to 7wt% (~6 kPa) (Fig 2D). Although, increasing the matrix
467 stiffness did not significantly impact the formation efficiency of EEOs in synthetic gels (Fig 2F-
468 G), decreasing stiffness improved EEO morphology (Fig S4A) to match to those generated in
469 Matrigel, suggesting that EEO clonal growth is robust across a range of physical properties (Fig
470 2E-G; Fig S3). Moreover, we evaluated formulations that probed the molecular (adhesion
471 ligands) properties of the synthetic matrix using the dual-peptide approach. In agreement with
472 our previous work, hydrogel functionalization with GFOGER, but not PHSRN-K-RGD, was
473 necessary to robustly generate scEEOs in synthetic hydrogel (Fig 2C; Fig S3B). However,
474 quantification of EEO diameter distribution and total EEO count across different dual-peptide
475 'MIX' formulations showed comparable scEEO formation efficiency compared to GFOGER
476 alone or Matrigel (Fig 2F-G).
477 In the synthetic matrix, scEEOs retained proper polarity based on basolateral LMN
478 deposition and apical F-actin accumulation, like EEOs cultured in Matrigel and epithelial glands
479 *in vivo* (Fig 2H). Moreover, scEEOs in both synthetic gel and Matrigel maintained epithelial
480 marker expression and mitotic activity similar to the native endometrial glands (Fig S4B-C) and
481 sustained the capacity for hormone response based on expression of both estrogen receptor
482 (ESR) and progesterone receptor (PGR) (Fig 2I-J). Further confirmation of the maturity of EEOs
483 revealed distinct populations of motile ciliated and secretory epithelial cell that is comparable to
484 *ex vivo* endometrial glands (Fig S4D, Video 1). These results were consistent across several
485 tissue donors (N=10) and justified the use of soft hydrogels (3wt%) functionalized with
486 GFOGER alone or dual presentation of GFOGER and PHSRN-K-RGD (MIX) in further
487 experiments (Fig S3).
488
489 *3.2.2. Establishment and characterization of ESC cultures in synthetic hydrogel*

490 Following an analogous approach, the biomolecular and biophysical properties impacting
491 ESC culture in 3D were evaluated (Fig 3A). ESCs were viable for at least 15 days of culture in a
492 wide range of hydrogel conditions but demonstrated enhanced ECM remodeling capacity in
493 softer hydrogel microenvironments (Fig 3B-D). Although all integrin ligands formulations
494 supported ESC culture, hydrogels containing PHSRN-K-RGD demonstrated a modest increase
495 in remodeling and overall stromal growth compared to matrices containing GFOGER alone (Fig
496 3E-F).
497 Stromal reproductive function was experimentally assessed by maintaining 3D cultures for a
498 period 15 days, under sex hormone stimulation. In response to estrogen and a synthetic
499 progestin treatment (E_2 and MPA), ESCs underwent decidualization, a differentiation process
500 necessary for the establishment of pregnancy, characterized by the secretion of pro-gestational
501 protein prolactin (PRL) and morphological changes toward a round, polyploid decidual cell[67].
502 Although increased stiffness impacted ESC morphology and remodeling capacity, it did not alter
503 ESC hormone response (Fig 3G). However, ESC decidualization response could be significantly
504 suppressed by hormone treatment and inflammatory challenges (Fig 3H). Taken together, these
505 results suggest that a softer and more physiologically relevant (3wt% PEG) synthetic matrix
506 functionalized with GFOGER and PHSRN-K-RGD could support simultaneous culture of EEOs
507 and ESCs in a multi-cellular model of the human endometrium.
508
509 *3.2.3. Engineered synthetic matrices support stable co-culture of EEO and ESC with physiologic*
510 *function*
511 In the native endometrium both stromal and epithelial cells express hormone receptors,
512 including PGR and ESR, and mediate tissue-level reproductive function via direct and indirect
513 mechanisms involving multi-cellular communication.[68,6970,71] To generate a model capable of
514 reproducing and studying these complex biological phenomena *in vitro*, the synthetic matrix
515 formulation developed above was implemented to simultaneously culture matched EEOs and
516 ESCs under a fully defined common media for up to 15 days (Fig 4A, Video 4). Co-cultures
517 were exposed to hormone stimulation designed to mimic the proliferative (E_2, 'E'), secretory (E_2
518 + MPA, 'PE'), or menstrual (72 hr PE withdrawal + RU-486, 'W') phases of the idealized human
519 menstrual cycle (Fig 4C-D). All cultures were viable throughout the length of the experiments as
520 demonstrated by live/dead staining (Fig S9) and a proliferative profile (Fig 6G). Immunostaining
521 demonstrated the persistence of morphologically well-defined stromal and epithelial populations
522 (Fig 4B, Video 2-3). Changes in EEO morphology characterized by thickening of the pseudo-
523 stratified columnar epithelial layer and increased epithelial invaginations (Fig 4E, 5B) were

524 evident in the secretory phase cultures, and mimicked the structural development of endometrial
525 glands observed *in vivo* (Fig 5A). Bulk RNA sequencing (RNAseq) analysis demonstrated that
526 co-cultures were transcriptionally distinct from either ESC or EEOs cultured alone (Fig S6).
527 Further analysis revealed that the treatment groups reproduced hallmark pathways associated
528 with their respective menstrual phases (Fig 4F-H, S7). Under secretory phase conditions, a
529 robust stromal decidualization response was observed. Specially, progesterone-induced gene
530 expression, including PRL and ECM proteins, were significantly upregulated and cytokine-
531 mediated inflammatory signaling were downregulated in PE treated groups (Fig 4F-H).
532 Furthermore, canonical menstruation-associated pathways, including hypoxia[72], inflammation[68]
533 and coagulation[73] were also recapitulated in the withdrawal treatment group compared to E or
534 PE. (Fig S7C-E).
535 Next, we utilized functional assays to validate the co-culture menstrual model. Co-cultures
536 underwent decidualization, characterized by the secretion of PRL, in secretory groups, but was
537 suppressed in the menses groups (Fig 5C-D). Further, progestin treatment resulted in both
538 epithelial and stromal reduction in PGR staining not observed in the proliferative phase groups
539 (Fig 5E). Epithelial-specific hormone response was demonstrated by secretion of progestogen
540 associated endometrial protein (PAEP), a marker of the secretory epithelium (Fig 5F, S7). Co-
541 cultures also showed a significant increase of apoptosis in the menses groups compared to the
542 secretory treated groups supportive of the cell death observed during menstruation (Fig 5G-H,
543 S8). Finally, protein secretion profiles of matrix metalloproteinases (MMPs) were measured from
544 the spent media (Fig 5I, S13A) and recapitulated the remodeling dynamic changes observed *in*
545 *vivo.*[68,74] Altogether, this data demonstrates the development of a (I) fully defined and modular
546 synthetic ECM that supports a long term, stable co-culture of EEOs and ESCs, and (II) an *in*
547 *vitro* model of the cycling endometrium that is hormone responsive and recapitulates the
548 phenotypic, morphologic, and biochemical changes associated with the idealized human
549 menstrual cycle.
550
551 **3.3 Inflammation disrupts endometrial function via a stromal dominant form of cellular**
552 **communication**
553 Chronic overexpression of pro-inflammatory cytokines such as tumor necrosis factor alpha
554 (TNFα), and interleukin 1 beta (IL-1β) have been associated with reproductive diseases[75–77].
555 Here, the endometrial co-culture models were used to examine inflammation-mediated
556 disruption of endocrine function in the cycling endometrium. Proliferative, secretory, or menses
557 co-cultures were exposed to a continuous dose of IL1β (1 ng/mL) throughout the 15-day

558 experiment (Fig 4D). Progesterone action was significantly impaired in the co-cultures as
559 demonstrated by the loss of PGR expression (Fig 6F), and the complete inhibition of stromal
560 decidualization (Fig 5C). Although under inflammatory conditions ESC proliferation was
561 suppressed (Fig 6G), ESCs remained active and developed an elongated morphology in 3D
562 (Fig S10, Video 4) characterized by increased stromal remodeling and MMP activity (Fig 6D-E,
563 Fig S13). Furthermore, columnar epithelial cell morphology was significantly disrupted, resulting
564 in a thinner epithelial architecture (Fig 6B-C) reminiscent of the wound healing phenotype
565 described in other epithelial cell populations.[79] Bulk transcriptomic data and multiplex protein
566 analysis of secreted protein revealed a global up-regulation of pro-inflammatory cytokines and
567 down regulation of anti-inflammatory cytokines in the inflamed cultures (Fig S11). Principal
568 component analysis (PCA) and unsupervised hierarchical cluster analysis indicated clear
569 separation between inflamed cultures and engagement of pathways associated with
570 endometriotic diseases (Fig S13B).
571 To better understand the role of inflammation in disease progression we functionally
572 examined viability, growth rates and proliferation in co-cultures and monocultures. In co-
573 cultures, inflammation resulted in a significant increase EEO growth rate and subsequent decay
574 compared to the EEO-monoculture controls (Fig 6I, S12) suggesting that epithelial response to
575 inflammation is partially mediated by the stroma. To functionally characterize this behavior, we
576 examined the proliferative profile of these cultures. We identified that IL-1β significantly
577 suppressed stromal proliferation, but had no impact on EEO proliferation when cultured
578 separately. However, when co-cultured, IL-1β significantly increased EEO proliferation (Fig 6G-
579 H). A sharp growth and decay rates observed in the inflamed epithelium in the co-cultures was
580 attributed to increased cell death and apoptosis in the IL-1β treated groups (Fig S8, S9).
581 Transcriptomic analysis of revealed more differential gene expression in co-cultures compared
582 to monocultures, suggesting that the presence of both cell types enhance the response to
583 cytokine challenge. Altogether, these results support that inflammatory and progesterone signal
584 in the endometrium are primarily mediated via the stroma in both physiologic and pathologic
585 conditions (Fig 6J). These findings demonstrate a platform that can recapitulate progesterone's
586 mechanisms of action in the endometrium[70,80] and dissects the mechanisms driving reproductive
587 disease pathogenesis.

588 **Discussion:**

589 In the human endometrium, rapid spatial and temporal changes, primarily driven by E2 and
590 P4, induce rapid alterations to ECM properties that are mechanically and molecularly linked to
591 reproductive function.[81] Tunable and bio-labile synthetic matrices that capture these dynamic
592 ECM properties are required to dissect the mechanisms driving tissue function and disease
593 pathogenesis.[82] Hydrogels are well suited for 3D cell culture due to their ability to mimic the
594 architecture and composition of the ECM. Matrigel, a heterogenous mixture of reconstituted
595 basement membrane proteins, provides an efficient, yet restrictive, substrate to establish,
596 expand, and study endometrial epithelial cells as organoids. The limitations of Matrigel have
597 been thoroughly described elsewhere.[21,83] Briefly, the variability of its composition, limited
598 tunability and presence of xenogeneic contaminants severely impact its applications for multi-
599 cellular models and translational research. Synthetic ECMs enable the tailoring the biophysical
600 and molecular properties to mimic those of the native tissue[25,81,84]. In this report, we used a
601 multi-omic deconstructive approach to explore synthetic matrix regimes that closely simulated
602 those of the native endometrial tissue and established a synthetic ECM that supports a multi-
603 cellular *in vitro 3D* model of the human menstrual cycle.

604 Though efforts to generate Matrigel alternatives to culture endometrial cells have been
605 presented[85–89], we report a fully synthetic hydrogel formulation that supports the long-term
606 embedded culture of both primary EEOs and ESCs in 3D. Our previous work using endometrial
607 cell lines identified that the fibronectin-mimetic (PHSRN-K-RGD) peptide supported the culture
608 of endometrial fibroblasts in a synthetic hydrogel.[26] More recently, we reported the generation of
609 epithelial organoids using the collagen-derived adhesion peptide GFOGER.[27] Here, we
610 corroborated these findings and tailored the matrix to enable co-cultures of these cell
611 populations that can mimic the idealized phases of the human menstrual cycle. By targeting the
612 α2β1 and α5β1 integrins expressed by the epithelial and stromal cells, respectively, with both
613 GFOGER and PHSRN-K-RGD (MIX) we observed improved scEEO formation efficiency (70.6 ±
614 13.2%) compared to the GFOGER-only matrices (49.3 ± 15.31%) (Fig 2F-G). These results
615 corroborated our previous findings[26,27,90] that focused on relatively stiff PEG hydrogels (> 2 kPa)
616 that are drastically different than the native endometrium (~250 Pa[65]) or of Matrigel of (~150-443
617 Pa).[21,66] By modulating the total PEG concentration (wt%), while maintaining consistent
618 crosslinking (45%) to more closely mimic the native ECM, we identified that decreasing hydrogel
619 stiffness (3wt%, ~300 Pa) further improved the scEEO forming efficiency in both the MIX (77.7 ±
620 16.3%) or GFOGER-only formulations (64.9 ± 16.7%). Changing the elastic moduli of the tissue
621 environment, either approaching or moving away from those of native tissues, can lead to

622 tremendous differences in cellular responses.[81,84] We identified that stiffer ECM regimes (5wt%,
623 ~2 kPa; 7wt%, ~6 kPa) strongly impacted EEO morphology and ESC remodeling compared to
624 softer matrices. Robust stromal stellate spreading, and spherical organoid morphology was
625 consistently maintained in the 3wt% hydrogels (Fig S2). Although hydrogel stiffness altered
626 EEO morphology, organoid generation and diameter was not significantly impacted (Fig 2F-G).
627 Moreover, we demonstrated a significant increase in stromal decidualization when cultured in
628 3D compared to 2D cultures, a finding whose mechanisms will require further investigation, yet
629 may impact the future of culture and analysis of *in vitro* endometrial stromal cells (Fig 3G). To
630 physiologically model the endometrium, we focused on the soft (3 wt%) hydrogels to generate
631 the co-cultures, however, these stiffness-mediated phenotypes may provide insight into cell-
632 ECM interactions in endometriotic diseases.[91] We conclude that the dual-peptide 3wt%-MIX
633 formulations is a novel approach to generate a synthetic matrix that is suitable for the culture of
634 both the epithelial and stromal cells either as mono- or co-cultures. To test the efficacy of the
635 synthetic matrix, we validated that expansion of scEEOs from original primary tissue is feasible
636 in the synthetic ECM without the need to first expand in Matrigel (Fig S14). This confers the
637 opportunity to investigate epithelial cell function otherwise masked by exogenous cytokines and
638 growth factors found in Matrigel.
639 Numerous approaches to generate *in vitro* models of the endometrial microenvironment that
640 attempt to dissect the intercellular communication that regulate reproductive function and
641 disease have been reported. These models include de-cellularized scaffolds[30,92], explant tissue
642 models[29,31,88,93], microfluidic organ-on-chip approaches[94–96] and 3D culture models.[26,29,30] Of
643 these, renal graft models have been particularly useful in elucidating mechanisms by which
644 hormones regulate epithelial and stromal function in the endometrium[70,71,97,98], yet their technical
645 complexity and limited human translation make them challenging models to interpret and
646 reproduce.[44,70] Here, we report a modular, tunable, and scalable 3D *in vitro* human alterative
647 that similarly captures tissue-level cellular communication, but enables a more robust analytical
648 capability (Fig 6). To appropriately dissect stromal-epithelial communication, we defined
649 stromal-epithelial cell ratios that were shown to approximate those observed *in vivo* (Fig S6).
650 Key reproductive events such as tissue regeneration, embryo implantation and menstruation
651 are all meditated by inflammatory mediators such as cytokines, chemokines, and prostaglandins
652 that regulate tissue function via cell-mediated communication[1,31,99]. However, uncontrolled
653 inflammation may promote the development of reproductive diseases such as endometriosis,
654 infertility, and abnormal menstrual bleeding. Endometriosis is a reproductive disorder
655 histologically characterized by the ectopic growth of endometrial tissue[9] and is closely

656 associated with pro-inflammatory mediators such as TNFα and IL1β as part of its pathogensis.[75]
657 Using the co-culture model of the cycling endometrium described, we demonstrated that
658 exogenous stimulation by IL1β recapitulated hallmarks of the endometriotic phenotype (Fig 6).
659 As expected, reduced P4 sensitivity was observed in the inflamed co-cultures system, reflected
660 by a complete loss of stromal decidualization (Fig 5C), increased epithelial growth (Fig 6G-H),
661 and induction of additional pro-inflammatory cytokines (Fig S11). We observed that
662 inflammation significantly reduced proliferation in the ESC, but increased matrix remodeling and
663 induced an elongated morphology, suggestive of a fibrotic response[100]. Likewise, epithelial cells
664 underwent a morphologic change from a mature columnar epithelial structure to a thin
665 squamous morphology in response to inflammation, suggestive of an wound healing
666 phenotype[79]. Together, these results demonstrate an altered cellular phenotype in the stromal
667 and epithelial compartments due to inflammation may be closely linked to the invasive
668 phenotype and fibrotic environment associated with endometriotic disease[101–103]. Moreover, by
669 examining the mitogenic effects of sex hormones and inflammation in our co-culture system, we
670 demonstrate the novel mechanistic finding that inflammation does not impacts epithelial
671 proliferation, differentiation, and function, but is mediated through the stromal fibroblasts (Fig
672 6J). Though intended as a proof of concept to demonstrate the capacity to dissect the
673 mechanisms of cell-cell communication, the cell-specific mediators will warrant further analysis
674 to identify the molecular factors driving this cellular response.
675 Altogether, this model provides a user-friendly and reproducible screening tool to explore
676 the endocrine-mediated axis of cell-cell communication using organoid technologies that is
677 amenable for therapeutic and contraceptive drug testing. Our approach to utilize pharmacologic
678 PGR antagonists (RU-486) to induce menstruation supports the ability to examine clinical
679 applications of selective hormone receptor modulators. Although this model robustly examines
680 the role of the epithelial and stromal compartments, it is important to consider the role of other
681 cell populations of the endometrial microenvironment, such as endothelial[90] and immune cells,
682 to support reproductive function or pathogenesis. The modular and tunable nature of this 3D
683 hydrogel platform makes the endometrial co-culture model is amenable for microfluidic and
684 organ-on-chip applications to incorporate these other cell populations.
685

686 **Acknowledgements:** We thank the Newton Wellesley Hospital staff for facilitating a tissue
687 collection program with MIT and the patients that donated their tissues for our research. We
688 thank Histology Facility at the Koch Institute at MIT for their assistance with histological
689 processing of tissues. We thank Prof. Kevin Osteen and Kaylon Bruner-Tran at Vanderbilt
690 University for their guidance. J.S.G. was supported by an Environmental Toxicology Training
691 Grant (NIH T32 ES007020). This work was supported in part by funding from a Bill and Melinda
692 Gates, The John and Karine Begg Foundation, the Manton Foundation, and NIH U01
693 (EB029132).
694
695 **Author Contributions:** J.S.G. and A.T.B. conceived the study, designed, performed, and
696 analyzed the experiments. J.S.G. wrote the manuscript. J.S.G isolated, cultured and maintained
697 primary cell populations with the help of C.I. and L.B. In Vitro culture data processing and
698 analysis was performed by J.S.G., A.T.B., and K.B. Hydrogel and tissue biobank was
699 maintained by V.H.G, and C.I. Ex Vivo data processing and analysis was performed by B.G.
700 and L.B. for scRNAseq and proteomics, respectively. All were involved in editing the
701 manuscript. M.L., K.I., and J.S.G. supervised tissue collection. L.G.G. supervised project
702 development and edited the manuscript.
703
704 **Competing Interests statement:** L.G.G. and V.H.G. have a patent application pending related
705 to the hydrogel system. The rest of the authors have no competing interests.
706
707 **Data availability**. Source data are available upon request from the corresponding author.

708 **4. References:**

709

710 1. Aplin J. Cellular biochemistry of the endometrium. *Biol Uterus*. 1989.

711 2. Aplin JD, Ruane PT. Embryo-epithelium interactions during implantation at a glance. *J Cell*
712 *Sci*. 2017;130(1):15-22. doi:10.1242/jcs.175943

713 3. Aplin JD. Cellular Biochemistry of the Endometrium. In: *Biology of the Uterus*. Vol 20.
714 Karger Publishers; 1989:89-129. doi:10.1007/978-1-4684-5589-2_6

715 4. Noyes R, Hertig A, Rock J. Dating the endometrial biopsy. *Obstet Gynecol ….* 1950.

716 5. Loy SLY and TS. Normal cycling Endometrium:Molecular, Cellular, and Histologic
717 Perspectives. In: *Endometriosis in Clinical Practice*. ; 2005:1-29.

718 6. Roy A, Matzuk MM. Reproductive tract function and dysfunction in women. *Nat Rev*
719 *Endocrinol*. 2011;7(9):517-525. doi:10.1038/nrendo.2011.79

720 7. Brosens JJ, Hayashi N, White JO. Progesterone receptor regulates decidual prolactin
721 expression in differentiating human endometrial stromal cells. *Endocrinology*.
722 1999;140(10):4809-4820. doi:10.1210/endo.140.10.7070

723 8. Kelleher AM, Demayo FJ, Spencer TE. Uterine Glands: Developmental Biology and
724 Functional Roles in Pregnancy. *Endocr Rev*. 2019;40(5):1424-1445. doi:10.1210/er.2018-
725 00281

726 9. Cameron IT, Fraser IS, Smith SK (Stephen K. *Clinical Disorders of the Endometrium and*
727 *Menstrual Cycle*. Oxford University Press; 1998.

728 10. Clevers H. Modeling Development and Disease with Organoids. *Cell*. 2016;165(7):1586-
729 1597. doi:10.1016/j.cell.2016.05.082

730 11. Boretto M, Maenhoudt N, Luo X, et al. Patient-derived organoids from endometrial disease
731 capture clinical heterogeneity and are amenable to drug screening. *Nat Cell Biol*.
732 2019;21(8):1041-1051. doi:10.1038/s41556-019-0360-z

733 12. Turco MY, Gardner L, Hughes J, et al. Long-term, hormone-responsive organoid cultures
734 of human endometrium in a chemically defined medium. *Nat Cell Biol*. 2017;19(5):568-577.
735 doi:10.1038/ncb3516

736 13. Boretto M, Cox B, Noben M, et al. Development of organoids from mouse and human
737 endometrium showing endometrial epithelium physiology and long-term expandability.
738 *dev.biologists.org*. 2017. doi:10.1242/dev.148478

739 14. Sato T, Stange DE, Ferrante M, et al. Long-term expansion of epithelial organoids from
740 human colon, adenoma, adenocarcinoma, and Barrett's epithelium. *Gastroenterology*.
741 2011;141(5):1762-1772. doi:10.1053/j.gastro.2011.07.050

742 15. Fujii M, Matano M, Toshimitsu K, et al. Human Intestinal Organoids Maintain Self-Renewal
743 Capacity and Cellular Diversity in Niche-Inspired Culture Condition. *Cell Stem Cell*.
744 2018;23(6):787-793.e6. doi:10.1016/j.stem.2018.11.016
745 16. Fitzgerald HC, Dhakal P, Behura SK, Schust DJ, Spencer TE. Self-renewing endometrial
746 epithelial organoids of the human uterus. *Proc Natl Acad Sci U S A*. 2019;116(46):23132-
747 23142. doi:10.1073/pnas.1915389116
748 17. Nakamura T, Sato T. Advancing Intestinal Organoid Technology Toward Regenerative
749 Medicine. *CMGH*. 2018;5(1):51-60. doi:10.1016/j.jcmgh.2017.10.006
750 18. Cruz-Acuña R, Quirós M, Farkas AE, et al. Synthetic hydrogels for human intestinal
751 organoid generation and colonic wound repair. *Nat Cell Biol*. 2017;19(11):1326-1335.
752 doi:10.1038/ncb3632
753 19. Sato T, Vries RG, Snippert HJ, et al. Single Lgr5 stem cells build crypt-villus structures in
754 vitro without a mesenchymal niche. *Nature*. 2009;459(7244):262-265.
755 doi:10.1038/nature07935
756 20. Talbot NC, Caperna TJ. Proteome array identification of bioactive soluble proteins/peptides
757 in Matrigel: relevance to stem cell responses. *Cytotechnology*. 2015;67(5):873-883.
758 doi:10.1007/s10616-014-9727-y
759 21. Hughes CS, Postovit LM, Lajoie GA. Matrigel: a complex protein mixture required for
760 optimal growth of cell culture. *Proteomics*. 2010;10(9):1886-1890.
761 doi:10.1002/pmic.200900758
762 22. Cruz-Acuña R, García AJ, Cruz-Acuna R, Garcia AJ, Cruz-Acuña R, García AJ. Synthetic
763 hydrogels mimicking basement membrane matrices to promote cell-matrix interactions.
764 *Matrix Biol*. 2017;57-58:324-333. doi:10.1016/j.matbio.2016.06.002
765 23. Capeling MM, Czerwinski M, Huang S, et al. Nonadhesive Alginate Hydrogels Support
766 Growth of Pluripotent Stem Cell-Derived Intestinal Organoids. *Stem Cell Reports*.
767 2019;12(2):381-394. doi:10.1016/j.stemcr.2018.12.001
768 24. Gjorevski N, Sachs N, Manfrin A, et al. Designer matrices for intestinal stem cell and
769 organoid culture. *Nat Publ Gr*. 2016;539(7630):560-564. doi:10.1038/nature20168
770 25. Kratochvil MJ, Seymour AJ, Li TL, Paşca SP, Kuo CJ, Heilshorn SC. Engineered materials
771 for organoid systems. *Nat Rev Mater*. 2019;4(9):606-622. doi:10.1038/s41578-019-0129-
772 9
773 26. Cook CD, Hill AS, Guo M, et al. Local remodeling of synthetic extracellular matrix
774 microenvironments by co-cultured endometrial epithelial and stromal cells enables long-
775 term dynamic physiological function. *Integr Biol (United Kingdom)*. 2017;9(4):271-289.

776 doi:10.1039/c6ib00245e
777 27. Hernandez-Gordillo V, Kassis T, Lampejo A, et al. Fully synthetic matrices for in vitro
778 culture of primary human intestinal enteroids and endometrial organoids. *Biomaterials*.
779 2020;254:120125. doi:10.1016/j.biomaterials.2020.120125
780 28. Pierro E, Minici F, Alesiani O, et al. Stromal-Epithelial Interactions Modulate Estrogen
781 Responsiveness in Normal Human Endometrium1. *Biol Reprod*. 2001;64(3):831-838.
782 doi:10.1095/biolreprod64.3.831
783 29. Arnold JT, Kaufman DG, Seppälä M, Lessey BA. Endometrial stromal cells regulate
784 epithelial cell growth in vitro: A new co-culture model. *Hum Reprod*. 2001;16(5):836-845.
785 doi:10.1093/humrep/16.5.836
786 30. Abbas Y, Brunel LG, Hollinshead MS, et al. Generation of a three-dimensional collagen
787 scaffold-based model of the human endometrium. *Interface Focus*. 2020;10(2):20190079.
788 doi:10.1098/rsfs.2019.0079
789 31. Osteen KG, Rodgers WH, Gaire M, Hargrove JT, Gorstein F, Matrisian LM. Stromal-
790 epithelial interaction mediates steroidal regulation of metalloproteinase expression in
791 human endometrium. *Proc Natl Acad Sci U S A*. 1994;91(21):10129-10133.
792 doi:10.1073/pnas.91.21.10129
793 32. Rezakhani S, Gjorevski N, Lutolf MP. Low-Defect Thiol-Michael Addition Hydrogels as
794 Matrigel Substitutes for Epithelial Organoid Derivation. *Adv Funct Mater*.
795 2020;30(48):2000761. doi:10.1002/adfm.202000761
796 33. Below CR, Kelly J, Brown A, et al. A microenvironment-inspired synthetic three-
797 dimensional model for pancreatic ductal adenocarcinoma organoids. *Nat Mater*. 2021.
798 doi:10.1038/s41563-021-01085-1
799 34. Osteen KG, Hill GA, Hargrove JT, Gorstein F. Development of a method to isolate and
800 culture highly purified populations of stromal and epithelial cells from human endometrial
801 biopsy specimens. *Fertil Steril*. 1989;52(6):965-972. doi:10.1016/S0015-0282(16)53160-4
802 35. Turco MY, Gardner L, Hughes J, et al. Long-term, hormone-responsive organoid cultures
803 of human endometrium in a chemically defined medium. *Nat Cell Biol*. 2017;19(5):568-577.
804 doi:10.1038/ncb3516
805 36. Turco MY, Gardner L, Kay RG, et al. Trophoblast organoids as a model for maternal–fetal
806 interactions during human placentation. *Nature*. 2018;564(7735):263-281.
807 doi:10.1038/s41586-018-0753-3
808 37. Lutolf MP, Lauer-Fields JL, Schmoekel HG, et al. Synthetic matrix metalloproteinase-
809 sensitive hydrogels for the conduction of tissue regeneration: Engineering cell-invasion

810 characteristics. *Proc Natl Acad Sci U S A*. 2003;100(9):5413-5418.
811 doi:10.1073/pnas.0737381100
812 38. Cambria E, Renggli K, Ahrens CC, et al. Covalent Modification of Synthetic Hydrogels with
813 Bioactive Proteins via Sortase-Mediated Ligation. *Biomacromolecules*. 2015;16(8):2316-
814 2326. doi:10.1021/acs.biomac.5b00549
815 39. Kuhlman W, Taniguchi I, Griffith LG, Mayes AM. Interplay between PEO tether length and
816 ligand spacing governs cell spreading on RGD-modified PMMA-g-PEO comb copolymers.
817 *Biomacromolecules*. 2007;8(10):3206-3213. doi:10.1021/bm070237o
818 40. Wojtowicz AM, Shekaran A, Oest ME, et al. Coating of biomaterial scaffolds with the
819 collagen-mimetic peptide GFOGER for bone defect repair. *Biomaterials*. 2010;31(9):2574-
820 2582. doi:10.1016/j.biomaterials.2009.12.008
821 41. Gao X, Groves MJ. Fibronectin-binding peptides. I. Isolation and characterization of two
822 unique fibronectin-binding peptides from gelatin. *Eur J Pharm Biopharm*. 1998;45(3):275-
823 284. doi:10.1016/S0939-6411(98)00010-1
824 42. Johnson G, Moore SW. Identification of a structural site on acetylcholinesterase that
825 promotes neurite outgrowth and binds laminin-1 and collagen IV. *Biochem Biophys Res*
826 *Commun*. 2004;319(2):448-455. doi:10.1016/j.bbrc.2004.05.018
827 43. Kurita T, Medina R, Schabel AB, et al. The activation function-1 domain of estrogen
828 receptor α in uterine stromal cells is required for mouse but not human uterine epithelial
829 response to estrogen. *Differentiation*. 2005;73(6):313-322. doi:10.1111/j.1432-
830 0436.2005.00033.x
831 44. Cunha GR, Baskin L. Use of sub-renal capsule transplantation in developmental biology.
832 *Differentiation*. 2016;91(4-5):4-9. doi:10.1016/j.diff.2015.10.007
833 45. Kassis T, Hernandez-Gordillo V, Langer R, Griffith LG. OrgaQuant: Human Intestinal
834 Organoid Localization and Quantification Using Deep Convolutional Neural Networks. *Sci*
835 *Rep*. 2019;9(1):12479. doi:10.1038/s41598-019-48874-y
836 46. Käll L, Storey JD, Noble WS. Non-parametric estimation of posterior error probabilities
837 associated with peptides identified by tandem mass spectrometry. *Bioinformatics*.
838 2008;24(16):42-48. doi:10.1093/bioinformatics/btn294
839 47. Oberg AL, Mahoney DW, Eckel-Passow JE, et al. Statistical analysis of relative labeled
840 mass spectrometry data from complex samples using ANOVA. *J Proteome Res*.
841 2008;7(1):225-233. doi:10.1021/pr700734f
842 48. Ritchie ME, Phipson B, Wu D, et al. limma powers differential expression analyses for RNA-
843 sequencing and microarray studies. *Nucleic Acids Res*. 2015;43(7):e47-e47.

844 doi:10.1093/nar/gkv007
845 49. Hughes TK, Wadsworth MH, Gierahn TM, et al. Second-Strand Synthesis-Based
846 Massively Parallel scRNA-Seq Reveals Cellular States and Molecular Features of Human
847 Inflammatory Skin Pathologies. *Immunity*. 2020;53(4):878-894.e7.
848 doi:10.1016/j.immuni.2020.09.015
849 50. Gierahn TM, Wadsworth MH, Hughes TK, et al. Seq-Well: A Portable, Low-Cost Platform
850 for High-Throughput Single-Cell RNA-Seq of Low-Input Samples. *Nat Methods*.
851 2017;14(4):395-398. doi:10.1038/nmeth.4179.Seq-Well
852 51. Robinson MD, McCarthy DJ, Smyth GK. edgeR: A Bioconductor package for differential
853 expression analysis of digital gene expression data. *Bioinformatics*. 2009;26(1):139-140.
854 doi:10.1093/bioinformatics/btp616
855 52. McCarthy DJ, Chen Y, Smyth GK. Differential expression analysis of multifactor RNA-Seq
856 experiments with respect to biological variation. *Nucleic Acids Res*. 2012;40(10):4288-
857 4297. doi:10.1093/nar/gks042
858 53. Zhang Y, Parmigiani G, Johnson WE. ComBat-seq: batch effect adjustment for RNA-seq
859 count data. *NAR Genomics Bioinforma*. 2020;2(3):1-10. doi:10.1093/nargab/lqaa078
860 54. Wang W, Vilella F, Alama P, et al. Single-cell transcriptomic atlas of the human
861 endometrium during the menstrual cycle. *Nat Med*. 2020;26(10):1644-1653.
862 doi:10.1038/s41591-020-1040-z
863 55. Lucas ES, Vrljicak P, Muter J, et al. Recurrent pregnancy loss is associated with a pro-
864 senescent decidual response during the peri-implantation window. *Commun Biol*.
865 2020;3(1):37. doi:10.1038/s42003-020-0763-1
866 56. O'Connor BB, Pope BD, Peters MM, Ris-Stalpers C, Parker KK. The role of extracellular
867 matrix in normal and pathological pregnancy: Future applications of microphysiological
868 systems in reproductive medicine. *Exp Biol Med*. 2020;245(13):1163-1174.
869 doi:10.1177/1535370220938741
870 57. Lessey BA, Damjanovich L, Coutifaris C, Castelbaum A, Albeida SM, Buck CA. Integrin
871 adhesion molecules in the human endometrium. Correlation with the normal and abnormal
872 menstrual cycle. *J Clin Invest*. 1992;90(1):188-195. doi:10.1172/JCI115835
873 58. Béliard A, Donnez J, Nisolle M, Foidart JM. Localization of laminin, fibronectin, E-cadherin,
874 and integrins in endometrium and endometriosis. *Fertil Steril*. 1997;67(2):266-272.
875 doi:10.1016/S0015-0282(97)81909-7
876 59. Bischof P, Redard M, Gindre P, Vassilakos P, Campana A. Localization of alpha 2, alpha
877 5 and alpha 6 integrin subunits in human endometrium, decidua and trophoblast. *Eur J*

878 *Obstet Gynecol Reprod Biol*. 1993;51(3):217-226. doi:10.1016/0028-2243(93)90038-E
879 60. Tabibzadeh S. Patterns of expression of integrin molecules in human endometrium
880 throughout the menstrual cycle. *Hum Reprod*. 1992;7(6):876-882.
881 doi:10.1093/oxfordjournals.humrep.a137753
882 61. Chen JI-C, Hannan NJ, Mak Y, et al. Proteomic Characterization of Midproliferative and
883 Midsecretory Human Endometrium. *J Proteome Res*. 2009;8(4):2032-2044.
884 doi:10.1021/pr801024g
885 62. Hood BL, Liu B, Alkhas A, et al. Proteomics of the Human Endometrial Glandular
886 Epithelium and Stroma from the Proliferative and Secretory Phases of the Menstrual
887 Cycle1. *Biol Reprod*. 2015;92(4). doi:10.1095/biolreprod.114.127217
888 63. Rai P, Kota V, Sundaram CS, Deendayal M, Shivaji S. Proteome of human endometrium:
889 Identification of differentially expressed proteins in proliferative and secretory phase
890 endometrium. *PROTEOMICS – Clin Appl*. 2010;4(1):48-59.
891 doi:https://doi.org/10.1002/prca.200900094
892 64. Valdez J, Cook CD, Ahrens CC, et al. On-demand dissolution of modular, synthetic
893 extracellular matrix reveals local epithelial-stromal communication networks. *Biomaterials*.
894 2017;130:90-103. doi:10.1016/j.biomaterials.2017.03.030
895 65. Abbas Y, Carnicer-Lombarte A, Gardner L, et al. Tissue stiffness at the human maternal-
896 fetal interface. *Hum Reprod*. 2019;34(10):1999-2008. doi:10.1093/humrep/dez139
897 66. Soofi SS, Last JA, Lliensiek SJ, Nealey PF, Murphy CJ. Elastic modulus of Matrigel as
898 determined by AFM. *J Struct Biol*. 2009;167(3):216-219.
899 doi:10.1016/j.jsb.2009.05.005.The
900 67. Wetendorf M, DeMayo FJ. The progesterone receptor regulates implantation,
901 decidualization, and glandular development via a complex paracrine signaling network. *Mol*
902 *Cell Endocrinol*. 2012;357(1-2):108-118. doi:10.1016/j.mce.2011.10.028
903 68. Critchley HO, Maybin JA, Armstrong GM, Williams ARW. Physiology of the endometrium
904 and regulation of menstruation. *Physiol Rev*. February 2020.
905 doi:10.1152/physrev.00031.2019
906 69. Mehasseb MK, Panchal R, Taylor AH, Brown L, Bell SC, Habiba M. Estrogen and
907 progesterone receptor isoform distribution through the menstrual cycle in uteri with and
908 without adenomyosis. *Fertil Steril*. 2011;95(7):2228-2235, 2235.e1.
909 doi:10.1016/j.fertnstert.2011.02.051
910 70. Cunha GR, Bigsby RM, Cooke PS, Sugimura Y. Stromal-epithelial interactions in adult
911 organs. *Cell Differ*. 1985;17(3):137-148. doi:10.1016/0045-6039(85)90481-6

912 71. Cooke PS, Buchanan DL, Young P, et al. Stromal estrogen receptors mediate mitogenic
913 effects of estradiol on uterine epithelium. *Proc Natl Acad Sci U S A*. 1997;94(12):6535-
914 6540. doi:10.1073/pnas.94.12.6535
915 72. Reavey JJ, Walker C, Nicol M, et al. Markers of human endometrial hypoxia can be
916 detected in vivo and ex vivo during physiological menstruation. *Hum Reprod*.
917 2021;36(4):941-950. doi:10.1093/humrep/deaa379
918 73. Davies J, Kadir RA. Endometrial haemostasis and menstruation. *Rev Endocr Metab*
919 *Disord*. 2012;13(4):289-299. doi:10.1007/s11154-012-9226-4
920 74. Bruner KL, Rodgers WH, Gold LI, et al. Transforming growth factor beta mediates the
921 progesterone suppression of an epithelial metalloproteinase by adjacent stroma in the
922 human endometrium. *Proc Natl Acad Sci U S A*. 1995;92(16):7362-7366.
923 75. Wang Y, Nicholes K, Shih IM. The Origin and Pathogenesis of Endometriosis. *Annu Rev*
924 *Pathol Mech Dis*. 2020;15:71-95. doi:10.1146/annurev-pathmechdis-012419-032654
925 76. Vercellini P, Viganò P, Somigliana E, Fedele L. Endometriosis: Pathogenesis and
926 treatment. *Nat Rev Endocrinol*. 2014;10(5):261-275. doi:10.1038/nrendo.2013.255
927 77. Horne AW, Saunders PTK. SnapShot: Endometriosis. *Cell*. 2019;179(7):1677-1677.e1.
928 doi:10.1016/j.cell.2019.11.033
929 78. Chan RWS, Lee CL, Ng EHY, Yeung WSB. Co-culture with macrophages enhances the
930 clonogenic and invasion activity of endometriotic stromal cells. *Cell Prolif*. 2017;50(3).
931 doi:10.1111/cpr.12330
932 79. Miyoshi H, VanDussen KL, Malvin NP, et al. Prostaglandin E2 promotes intestinal repair
933 through an adaptive cellular response of the epithelium. *EMBO J*. 2017;36(1):5-24.
934 doi:10.15252/embj.201694660
935 80. Cooke PS, Buchanan DL, Young P, et al. Stromal estrogen receptors mediate mitogenic
936 effects of estradiol on uterine epithelium. *Proc Natl Acad Sci U S A*. 1997;94(12):6535-
937 6540. doi:10.1073/pnas.94.12.6535
938 81. Griffith LG, Swartz MA. Capturing complex 3D tissue physiology in vitro. *Nat Rev Mol Cell*
939 *Biol*. 2006;7(3):211-224. doi:10.1038/nrm1858
940 82. Guimarães CF, Gasperini L, Marques AP, Reis RL. The stiffness of living tissues and its
941 implications for tissue engineering. *Nat Rev Mater*. February 2020:1-20.
942 doi:10.1038/s41578-019-0169-1
943 83. Aisenbrey EA, Murphy WL. Synthetic alternatives to Matrigel. *Nat Rev Mater*.
944 2020;5(7):539-551. doi:10.1038/s41578-020-0199-8
945 84. Nicolas J, Magli S, Rabbachin L, Sampaolesi S, Nicotra F, Russo L. 3D Extracellular Matrix

946 Mimics: Fundamental Concepts and Role of Materials Chemistry to Influence Stem Cell
947 Fate. *Biomacromolecules*. 2020;21(6):1968-1994. doi:10.1021/acs.biomac.0c00045
948 85. Francés-Herrero E, Juárez-Barber E, Campo H, et al. Improved models of human
949 endometrial organoids based on hydrogels from decellularized endometrium. *J Pers Med*.
950 2021;11(6). doi:10.3390/jpm11060504
951 86. López-Martínez S, Campo H, de Miguel-Gómez L, et al. A Natural Xenogeneic Endometrial
952 Extracellular Matrix Hydrogel Toward Improving Current Human in vitro Models and Future
953 in vivo Applications. *Front Bioeng Biotechnol*. 2021;9(March):1-20.
954 doi:10.3389/fbioe.2021.639688
955 87. Zambuto SG, Clancy KBH, Harley BAC. A gelatin hydrogel to study endometrial
956 angiogenesis and trophoblast invasion. *Interface Focus*. 2019;9(5).
957 doi:10.1098/rsfs.2019.0016
958 88. Muruganandan S, Fan X, Dhal S, Nayak NR. Development of A 3D Tissue Slice Culture
959 Model for the Study of Human Endometrial Repair and Regeneration. *Biomolecules*.
960 2020;10(1):136. doi:10.3390/biom10010136
961 89. Gargus ES, Rogers HB, McKinnon KE, Edmonds ME, Woodruff TK. Engineered
962 reproductive tissues. *Nat Biomed Eng*. 2020;4(4):381-393. doi:10.1038/s41551-020-0525-
963 x
964 90. Brown A, He H, Trumper E, Valdez J, Hammond P, Griffith LG. Engineering PEG-based
965 hydrogels to foster efficient endothelial network formation in free-swelling and confined
966 microenvironments. *Biomaterials*. 2020;243:119921.
967 doi:10.1016/j.biomaterials.2020.119921
968 91. Gnecco JS, Brown AT, Kan EL, et al. Physiomimetic Models of Adenomyosis. *Semin*
969 *Reprod Med*. 2020;38(2-3):179-196. doi:10.1055/s-0040-1719084
970 92. Olalekan SA, Burdette JE, Getsios S, Woodruff TK, Kim JJ. Development of a novel human
971 recellularized endometrium that responds to a 28-day hormone treatment. *Biol Reprod*.
972 2017;96(5):971. doi:10.1093/BIOLRE/IOX039
973 93. Schäfer WR, Fischer L, Roth K, et al. Critical evaluation of human endometrial explants as
974 an ex vivo model system: A molecular approach. *Mol Hum Reprod*. 2011;17(4):255-265.
975 doi:10.1093/molehr/gaq095
976 94. Gnecco JS, Ding T, Smith C, Lu J, Bruner-Tran KL, Osteen KG. Hemodynamic forces
977 enhance decidualization via endothelial-derived prostaglandin E2 and prostacyclin in a
978 microfluidic model of the human endometrium. *Hum Reprod*. 2019;34(4):702-714.
979 doi:10.1093/humrep/dez003

980 95. Gnecco JS, Pensabene V, Li DJ, et al. Compartmentalized Culture of Perivascular Stroma
981 and Endothelial Cells in a Microfluidic Model of the Human Endometrium. *Ann Biomed Eng*.
982 2017;45(7):1758-1769. doi:10.1007/s10439-017-1797-5
983 96. Kimura H, Nakamura H, Akai T, et al. On-chip single embryo coculture with microporous-
984 membrane-supported endometrial cells. *IEEE Trans Nanobioscience*. 2009;8(4):318-324.
985 doi:10.1109/TNB.2009.2035275
986 97. Bigsby RM. Control of growth and differentiation of the endometrium: The role of tissue
987 interactions. In: *Annals of the New York Academy of Sciences*. Vol 955. ; 2002:110-117.
988 doi:10.1111/j.1749-6632.2002.tb02771.x
989 98. Buchanan DL, Setiawan T, Lubahn DB, et al. Tissue compartment-specific estrogen
990 receptor-α participation in the mouse uterine epithelial secretory response. *Endocrinology*.
991 1999;140(1):484-491. doi:10.1210/endo.140.1.6448
992 99. Evans J, Salamonsen LA, Winship A, et al. Fertile ground: Human endometrial
993 programming and lessons in health and disease. *Nat Rev Endocrinol*. 2016;12(11):654-
994 667. doi:10.1038/nrendo.2016.116
995 100. Kendall RT, Feghali-Bostwick CA. Fibroblasts in fibrosis: novel roles and mediators. *Front*
996 *Pharmacol*. 2014;5:123. doi:10.3389/fphar.2014.00123
997 101. Konrad L, Dietze R, Riaz MA, et al. Epithelial-Mesenchymal Transition in Endometriosis-
998 When Does It Happen? *J Clin Med*. 2020;9(6). doi:10.3390/jcm9061915
999 102. Vigano P, Candiani M, Monno A, Giacomini E, Vercellini P, Somigliana E. Time to redefine
1000 endometriosis including its pro-fibrotic nature. *Hum Reprod*. 2017;33(3):347-352.
1001 doi:10.1093/humrep/dex354
1002 103. Clancy KBH. Reproductive ecology and the endometrium: Physiology, variation, and new
1003 directions. *Am J Phys Anthropol*. 2009;140(SUPPL. 49):137-154. doi:10.1002/ajpa.21188
1004

1005 **5. Figure Legends**

1006

1007 **Figure 1. A tissue-inspired multi-omic approach elucidates the design parameters to**
1008 **engineer a fully synthetic PEG hydrogel for the endometrium.** (A) Representative histological
1009 hematoxylin and eosin (H&E) stained samples of the menstrual cycle phases. (B) Heatmap of
1010 proteomic analysis of the human endometrium showing ECM proteins (matrisome) across the
1011 menstrual cycle (n = 8 donors). Green, red and purple boxes highlight collagens, fibronectin, and
1012 laminins as dynamic proteins in the endometrium. (C) Dot plot analysis of specific integrins
1013 expression from single cell RNA-seq data (n = 6 donors, 6,659 cells). Examination of stromal and
1014 epithelial component integrin expression across the menstrual cycle (proliferative and secretory
1015 phases) Circle size and color indicate P-value and the means of the average expression value.
1016 (D) Schematic of the overall strategy to design and fabricate a synthetic ECM for the
1017 endometrium. 8-arm 20kDa PEG macromers are functionalized with cell matrix binders (FN,
1018 B.M.), integrin binder adhesion peptides, and polymerized with a protease-labile crosslinker.
1019 Conceptual schematic of the dual-peptide hydrogel design to support multiple cell types and
1020 descriptive outline of the key peptides utilized to interact with integrins.

1021

1022 **Figure 2. Dual-peptide functionalization and softer synthetic matrix regimes enhance EEOs**
1023 **generation.** (A) Schematic of the workflow for identifying a synthetic hydrogel formulation for EEO
1024 generation from single cells. (B) Representative images of scEEO and morphology in stiff (5wt%)
1025 in soft (3wt%) PEG hydrogels functionalized with GFOGER (3mM) compared to Matrigel. (C) Day-
1026 15 images of hydrogel formulations comparing adhesion peptides reveals that GFOGER is
1027 necessary to generate scEEOs. Dual-peptide functionalization with GFOGER (1.5mM) and
1028 PHSN-K-RGD (1.5 mM) did not negatively affect scEEO generation. (D) Quantification of the
1029 biomechanical properties (elastic moduli, Pa, n=3 gels) of the synthetic hydrogel formulations.
1030 Soft = 3wt% (~300 pa), 5wt% = (~2kPa) and 7wt% (~6kPa). (E) Time-lapse images of 10-day
1031 cultures of EEO derived from single cells in synthetic hydrogels (PEG 3wt%-MIX). (F)
1032 Quantification of the total lumenized EEO (>100 um diameter) count and EEO diameter
1033 distribution (F) after 14 days of culture in different hydrogel formulation and in Matrigel. (G)
1034 Quantification of the scEEO forming efficiency in synthetic hydrogels relative to Matrigel (N=8).
1035 (H) Characterization of EEO morphology and polarity of EEOs generated in synthetic ECM (3wt%-
1036 MIX) compared to Matrigel via immunofluorescent (IF) analysis of ECM deposition (LMN) and F-
1037 actin accumulation. (I-J) Characterization of protein and transcriptomic expression of hormone
1038 receptors in EEOs generated in synthetic hydrogels. (I) Representative images of PGR staining
1039 and (J) qPCR analysis of mRNA expression of PGR and ESR in EEOs treated with either E_2 (E)
1040 or E_2 + MPA (EP) for 14 days. Analysis compares ESR, PGR values relative to matching E
1041 treatment groups (control).

1042

1043 **Figure 3. Development and characterization of a synthetic endometrial stromal cell culture.**
1044 (A) Schematic of the workflow for culturing ESCs in 3D using a synthetic hydrogel. (B) Time-
1045 lapse images of embedded ESCs in synthetic matrix allow for long-term stable cultures. (C-D)
1046 Representative images of 14-day old 3D cultures of ESC in the synthetic hydrogel comparing
1047 different adhesion peptides and stiffnesses. (D) Maximum intensity projection images of F-actin

1048 (green) reveal ESC remodeling (cell spreading) impacted primarily by hydrogel stiffness. (E-F)
1049 Representative 3D images and quantification (% fluorescence area) of ESC remodeling in
1050 synthetic ECMs. (G) Decidualization is not impacted by synthetic ECM (3wt% MIX). Biochemical
1051 measurement of prolactin (PRL) in the spent media from 14-day cultures treated with E_2 or E_2P4
1052 in synthetic hydrogels of different stiffnesses (3wt%, 5wt%, 7wt%) is significantly higher in 3D
1053 compared to 2D. (H) Inflammation (IL1β, 1 ng/mL) significantly suppressed decidualization in ESC
1054 cultures (E+ = E + IL1β, PE+= PE+IL1β, W = hormone withdrawal).
1055
1056 **Figure 4. Establishment and Establishment of a co-culture model recapitulate the**
1057 **molecular signature of the human menstrual cycle in vitro.** (A) Schematic and representative
1058 images of the co-cultures. EEOs (10 intact organoids/uL) and ESC (10k cells/uL) are expanded
1059 separately and embedded in the synthetic ECM and cultured as 3ul droplets for 15 days. A dual-
1060 peptide synthetic ECM (3wt% 20kDa-PEG) functionalized with GFOGER (1.5mM) and PHSRN-
1061 K-RGD (1.5mM) supports the establishment of the EEOs and ESC co-culture model. (B)
1062 Representative 3D images of day-15 endometrial EEOs (EpCAM = green) and ESC (Vimentin =
1063 red) in the co-cultures (scale =100 um). (C) Schematic and timeframe of the idealized 28-day
1064 menstrual cycle in vivo. (D) Experimental design for the validation of the co-culture endometrial
1065 model. Treatment groups are designed to mimic the hormonal changes in the phases of the
1066 menstrual cycle, including a pharmacologic induction of the menstruation using a PGR antagonist
1067 (RU-486, 10uM). Inflamed groups were co-treated with IL1β (1ng/mL) throughout the length of
1068 the experiment. (E) IF imaging of the co-cultures and characterization of morphologic changes in
1069 response to hormone treatment reveals epithelial maturation in response to progestin. (F-H)
1070 Transcriptomic (bulk RNAseq) analysis of the co-cultures models. (F) A heatmap using a curated
1071 list of menstrual genes clusters samples based on hormone treatment group. (G-H) Hallmark
1072 pathways show gene expression changes consistent with corresponding phases of the menstrual
1073 cycle. Gene ontology (GO) analysis of the top significantly enriched GO terms that are
1074 downregulated (G) or upregulated (H) in response to progesterone. Data is shown with the −log
1075 of their P values. Cocultures treated with E2 + MPA ("PE") have gene ontology (GO) expression
1076 profiles that align with the secretory phase of the menstrual cycle. All images and analysis were
1077 performed on day-15 co-cultures in the synthetic 3wt% 20kDa-PEG-Mix hydrogels (N=8).

1078 **Figure 5. Functional validation of the co-culture model recapitulates menstrual cycle-**
1079 **relevant reproductive processes.** (A) Representative histological (IF) characterization of the
1080 proliferative and secretory phases of the menstrual cycle reveals morphologic and biochemical
1081 changes. (B) 3D renderings of the co-culture recapitulate the morphological changes are
1082 observed in the secretory treated organoids. (C-D) Stromal decidualization was assessed by
1083 measuring prolactin secretion in the medium. (C) Temporal profiles of decidualization normalized
1084 to fold change relative to day 0) were performed by measuring spent media (N=12) and can be
1085 suppressed by IL1β treatment (1 ng/mL, E+, PE+). (D) PRL secretion is induced by PE treatment
1086 but suppressed in menses. (E) PGR staining in co-cultures at day 15 of treatment. (F) IF staining
1087 of PAEP (glycodelin) in co-cultures matches the epithelial secretory phenotype. (G-H) Cleaved
1088 caspase-3 (Casp-3) IF was performed in the cultures as a marker of apoptosis and quantified in
1089 (H). (I) MMPs were measured in the E vs PE co-cultures using a multiplex panel, day-15 MMP

1090 profiles is shown. All images are of day-15 co-cultures in the synthetic ECM 3wt% 20kDa-PEG-
1091 Mix hydrogels.

1092 **Figure 6. Functional analysis of inflammation in co-cultures in synthetic hydrogel reveals**
1093 **an endometriotic phenotype mediated by cell-cell communication.** (A) Live-dead 3D
1094 maximum intensity projections of co-cultures in the synthetic matrices in response to
1095 inflammation. (B-C) EEO morphology is impacted by inflammation. Representative images (B)
1096 and quantification (C) of epithelial thickness (N=3). (D-E) Representative IF images and
1097 quantification of the ESC morphology in the co-culture under inflamed and non-inflamed
1098 menstrual cycle conditions. (E) Increased ESC remodeling and decreased cell surface area was
1099 observed in in response to inflammation (N=3). (F) Day 15 PRL secretion is significantly inhibited
1100 in the inflamed groups. All images are of day-15 co-cultures in the synthetic ECM (3wt%-MIX).
1101 (G) Immunostaining analysis of the proliferative profiles of co-cultures and monocultures by EdU
1102 incorporation in response to hormones and inflammation (N=3). (H) Quantification of proliferative
1103 profiles calculated as a percentage of edu+, compared to DAPI stained nuclei for co-cultures and
1104 monocultures. (I) Real-time measurements of EEO diameter growth rates over 15 days (N=4) and
1105 quantified as fold change relative to the diameter from day 1 in control (E, PE, W) and inflamed
1106 (E+, PE+) conditions. (J) Conceptualization of the cellular mechanisms driving epithelial and
1107 stromal communication in the endometrium under physiologic (hormones) and pathogenic
1108 (inflamed) conditions. All images are of day-15 co-cultures in the synthetic ECM 3wt% 20kDa-
1109 PEG-Mix hydrogels.

1110

1111 **6. Supplementary Figures Legends:**

1112

1113 **Supplementary Fig 1. Characterization of the human endometrium using single cell**
1114 **transcriptomic analysis of the endometrium.** (A) Endometrial heterogeneity is shown as a t-
1115 distributed stochastic neighbor embedding (tSNE) projection colored by cell identities (left), and
1116 donor ID (top) and menstrual cycle stage (bottom). (B-C) Dot plot representation of the cycle
1117 phase dependent genes across the distinct cell populations (N=3). (C) Violin plots of the integrin
1118 expression across the endometrial cell populations (N=6). (D) Validation of cell specific integrin
1119 expression in cultured endometrial cells. ESC and EEOs were cultured in 2D in Matrigel
1120 respectively and analyzed by qPCR for integrin and hormone receptor expression relative to
1121 GAPDH (N=5).

1122 **Supplementary Fig 2. Workflow for EEO generation, hydrogel generation and screening.**
1123 (A) Schematic of primary endometrial tissue processing workflow to generate organoids (B) (D)
1124 Schematic of detailed EEO generation and hydrogel screening protocols.

1125 **Supplementary Fig 3. Screening and quantification of EEO generation in synthetic**
1126 **matrices across donors.** (A) Brightfield images of day-15 scEEO morphology cultured in
1127 hydrogel formulations. (B) Representative images of hydrogel screening of 5 different donors
1128 throughout the 14-day experiment derived from single cell. (C) Diameter of ten-day old
1129 endometrial organoids (n = 3 independent experiments) growing in the synthetic matrices
1130 described compared to EEOs cultured in Matrigel were quantified using a deep learning-algorithm
1131 (OrgaQuant) as described in the methods.

1132 **Supplementary Figure 4. Validation of EEOs cultured in PEG vs Matrigel.** (A) IF images of
1133 scEEO morphology derived in soft synthetic matrices compared to Matrigel. (B) Characterization
1134 of scEEOs reveal epithelial-origin in synthetic matrices and in Matrigel. (C) Ki67 staining of EEOs
1135 cultured in synthetic ECM and in Matrigel in addition to a 3D projection of KI67 stained ex vivo
1136 tissues. Inset is a gland cross-section. (D) Brightfield snaps from videos reflect epithelial
1137 heterogeneity and motile cilia. EEOs cultured in synthetic matrices and stained for acetylated a-
1138 tubulin reveal multi-ciliated and primary ciliated cells.

1139 **Supplementary Fig 5. Identifying cell ratios ex vivo for tissue modeling in vitro.** 3D imaging
1140 of ex vivo tissues using tissue clearing methods and confocal imaging were analyzed using the
1141 Imaris (Bitmap 9.6.0) software to segment the epithelial and stromal compartments of the native
1142 endometrium (N=3 donors, 3 different volumes) using the 'Surface' function to masks individual
1143 cell regions in a volumetric image. (A) The 'Cells' function Single cell segmentation tools from the
1144 software were utilized to calculate the number of epithelial cells (Epi) per volume of epithelial
1145 glands (Epi/μL). (B) ESC single cell counting in 3D was performed using the 'Spots' function by
1146 labeling and counting the DAPI+ nuclei in the image. A similar approach was taken for co-culture
1147 in vitro models. (C) Cell concentration per unit area the native endometrium and the cell ration
1148 between epithelial cells and stromal cells. (D) 3D analysis of EEOs cultured in the synthetic
1149 matrices. (E) Cell density in vivo and in vitro comparing relative numbers and epithelial cell gland

volumes. (F) No significant differences in the ratio between single ESCs concentration (ESC/µl) and Epithelial volume (gland/volume ratio).

Supplementary Fig 6. Establishment and transcriptomic analysis of monocultures and co-cocultures. (A) Representative brightfield images of co-culture (N=6) and monocultures of EEOs (N=1) and ESCs (N=6). (B) Unsupervised PCA analysis of bulk RNAseq co-cultures and monocultures cluster by culture type. Ellipses bound the 95% confidence interval for each group. **C)** Plotting $log_2(fold\ change)$ against -$log_{10}(P\ value)$ in a volcano plot shows differentially expressed genes in cocultures as compared to cultures of ESC only.

Supplementary Fig 1. Functional validation of endometrial-coculture recapitulation of the menstrual cycle in vitro. (A) Immunofluorescent images of the organoid morphology under 'proliferative (E)' and 'secretory (PE)' hormone treatment groups for both EEOs and ESC. Morphological assessment of altered cellular response to hormones and to inflammation (IL1β, 1ng/mL). (B) Immunofluorescent staining of PAEP of the day-15 co-cultures at a lower magnification reveals progesterone induced secretory phenotype in the EEOs. (C) Transcriptomic analysis of MMP reveals differential expression patterns in response to hormone treatments. (D-E) Gene Set Enrichment Analysis (GSEA) on a ranked list of genes from a generalized linear model of the coculture data. Hallmark pathways show gene expression changes consistent with corresponding phases of the menstrual cycle.

Supplementary Fig 2. Apoptosis is increased in the menstrual phase of the co-culture model and in the inflamed endometrium and corresponding viability is decreased in the inflamed group. (A-B) Comparison of apoptotic marker expression (cleaved caspase-3) immunofluorescent staining in co-cultures at day 15 in the menstrual cycle and inflamed groups in low (4X) and high (10X) magnification. (C) Quantification of ESC monoculture apoptosis relative to total nuclei count (N=3).

Supplementary Fig 9. Viability in the co-culture models at day 15. Low (4X) and high (10X) magnification of the Live (green) and Dead (red) assay in the hormone and inflammation and hormone treated groups comparing (A) cocultures and (B) ESC monocultures.

Supplementary Fig 10. Inflammation disrupts ESC remodeling and morphology. (A) Representative brightfield images of ESC monocultures in response to inflammation (IL1b, 1 ng/mL), reveals increased remodeling. (B) Immunofluorescent analysis of F-actin reveals morphologic changes associated with inflammatory response. Single cell segmentation (Red) elucidates the morphologic changes associated with hormone treatment and inflammation in 3D (N=3).

Supplementary Fig 11. Co-cultures treated with IL1β have transcriptomic profiles consistent with inflamed endometrial states. (A) A volcano plot of $log_2(fold\ change)$ against -$log_{10}(P\ value)$ for cocultures treated with inflammation as compared to non-inflamed controls. Transcript data is modeled using a generalized linear model to account for inter-donor and hormone treatment variability. (B) Differentially expressed genes were analyzed using gene ontology (GO) analysis to examine the most up- and down- regulated pathways. (C) A closer examination of the most significant GO terms reveals that canonical inflammatory genes are upregulated while PRL is

1190 downregulated, as expected for an inflamed environment. (D) Gene Set Enrichment Analysis
1191 (GSEA) on a ranked list of all expressed genes similarly shows an enrichment of inflammatory
1192 pathways upon IL1β treatment.

1193 **Supplementary Fig 12. Functional and molecular analysis of EEO growth rates.** Inflamed
1194 co-cultures and monocultures were analyzed to examine the growth rates of EEOs under
1195 hormone treatments. Daily images were analyzed to quantify the diameter fold change of the
1196 organoids relative to day 1 of cultures. Co-cultures revealed increased growth and decay rates in
1197 response to inflammation compared to mono-culture (EEO only) controls (N=6).

1198 **Supplementary Fig 13. Temporal validation of inflammatory response on co-cultures via**
1199 **functional and protein analysis.** Multiplex 45-panel of secreted cytokines measured in co-
1200 cultures throughout the 15-day experiment. Readings were measured every 3 days in control or
1201 inflamed conditions (N=3 replicates per day). (A) Daily changes in MMP panel protein secretion
1202 in co-cultures throughout the 15-day experiment. (B) Heatmap of temporal analysis of multiplex
1203 protein secretion. (C) Representative luminex panel of up regulated and downregulated cytokines
1204 in response to inflammation. Principal component analysis (PCA) and corresponding loading
1205 plots. All images are of day-15 co-cultures in the synthetic ECM (3wt%-MIX). (E = estradiol only,
1206 PE = E + MPA, M = PE withdrawal + RU486), E+ = E + IL1β, and PE+ = PE+IL1β, M+ = M +
1207 IL1β).

1208 **Supplementary Fig 14. EEOs can be generated and expanded directly into synthetic ECM**
1209 **from primary tissues.** (A) Schematic of epithelial gland collection and EEO generation and
1210 expansion using Matrigel and the synthetic matrix. (B) Brightfield images of EEOs generated in
1211 the synthetic matrix (3wt%-MIX) directly from freshly isolated gland fragments. (C)
1212 Characterization of Matrigel-free EEOs and immunofluorescent images of actin (green) staining.
1213 (D) Validation of expansion and passaging of EEOs (p1) using the synthetic matrix.

1214 **Supplementary Fig 15.** Histological metadata and characterization of endometrial tissues
1215 collected. (A) Hematoxylin and eosin stain (H&E) of endometrial tissues from endometrial tissues.
1216 (B) Table outlining patient metadata and tissue processing.

1217

1218 Graphical abstract

1219

1220

1221

1222

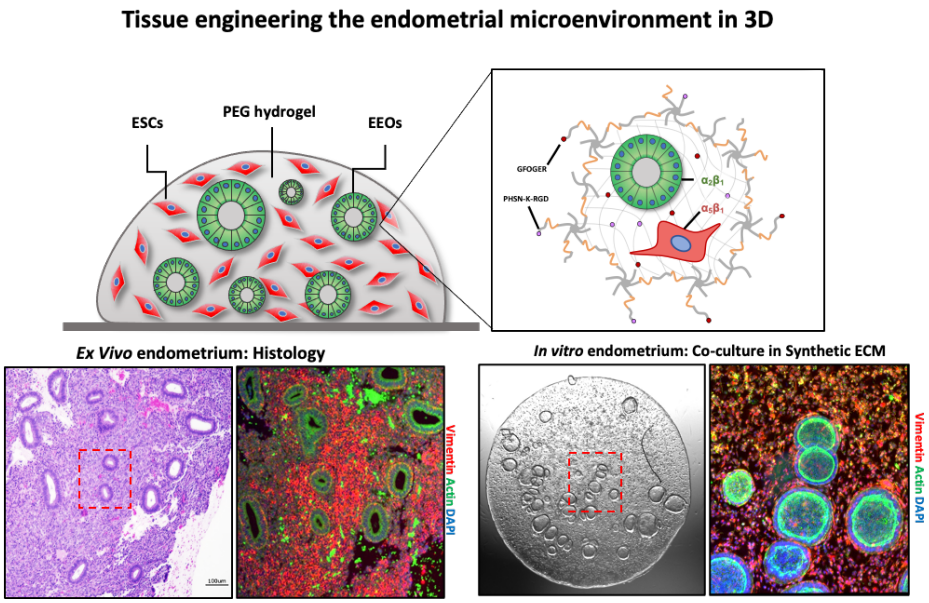

1223

Figure 1. A tissue-inspired multi-omic approach elucidates the design parameters to engineer a fully synthetic PEG hydrogel for the endometrium

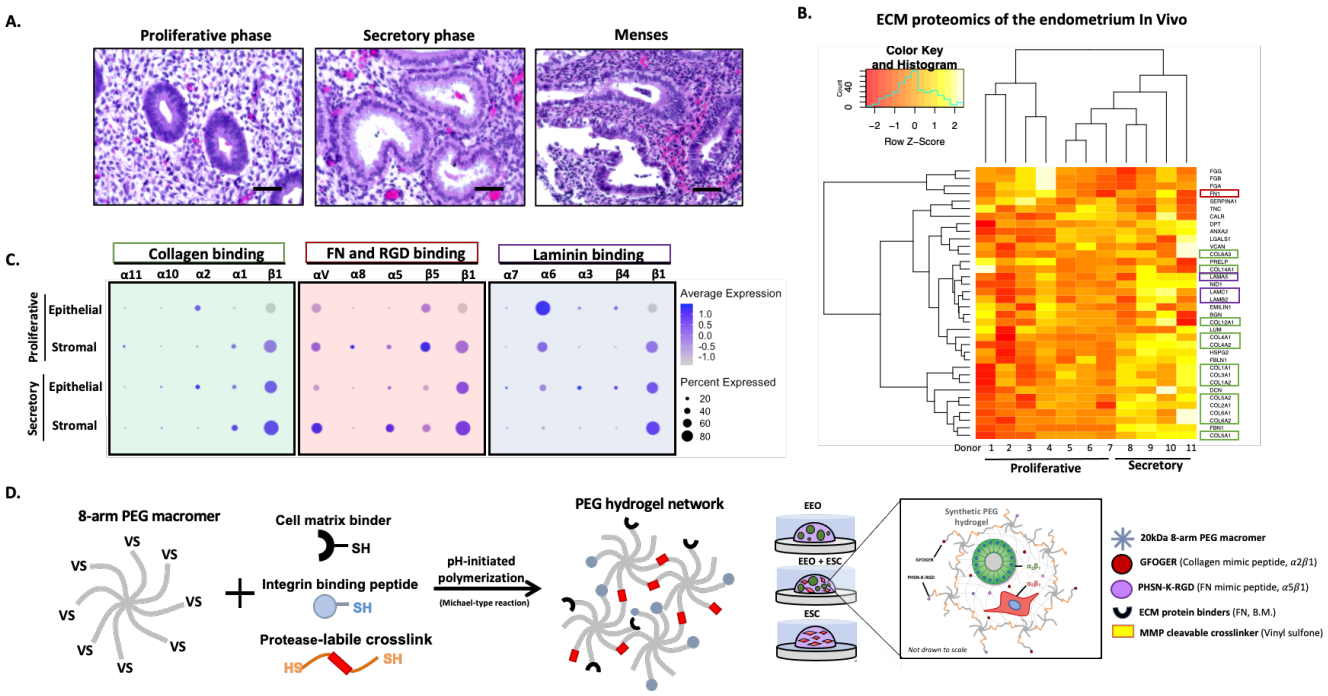

Figure 2. Dual-peptide functionalization and softer synthetic matrix regimes enhance EEOs generation.

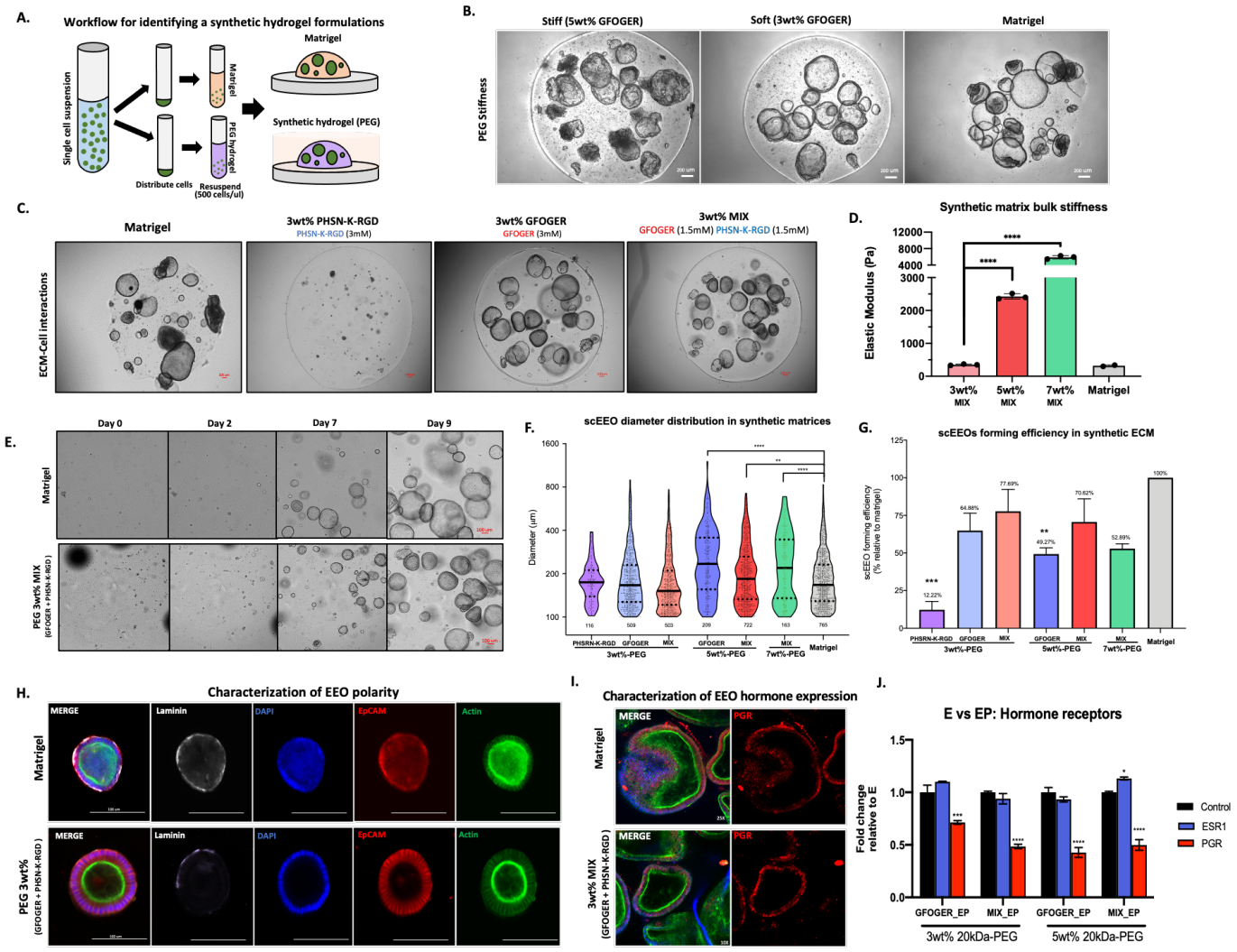

1236 **Figure 3. Development and characterization of a synthetic endometrial stromal cell**
1237 **culture.**
1238

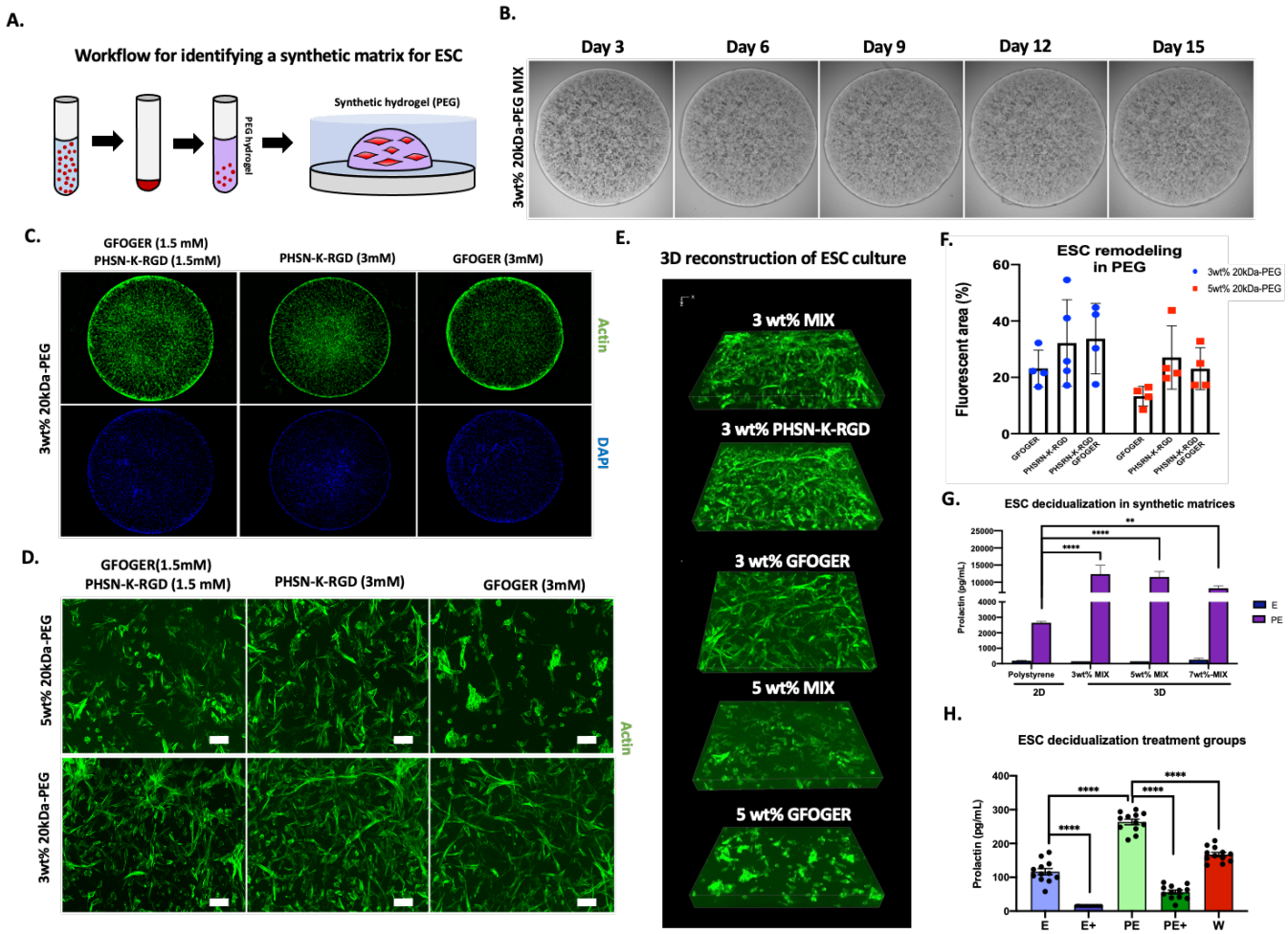

1239
1240

Figure 4. Establishment and Establishment of a co-culture model recapitulate the molecular signature of the human menstrual cycle in vitro.

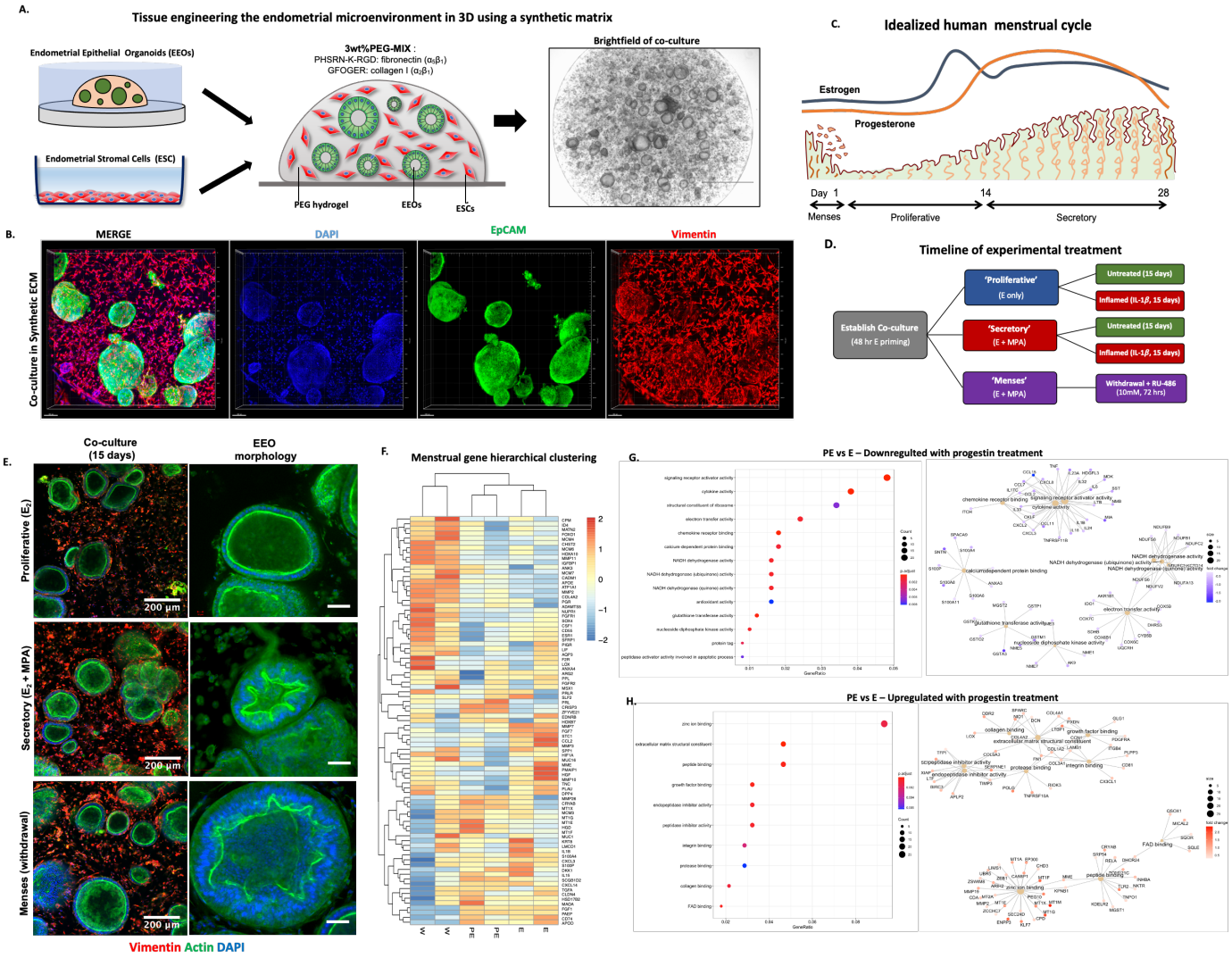

Figure 5. Functional validation of the co-culture model recapitulates menstrual cycle-relevant reproductive processes.

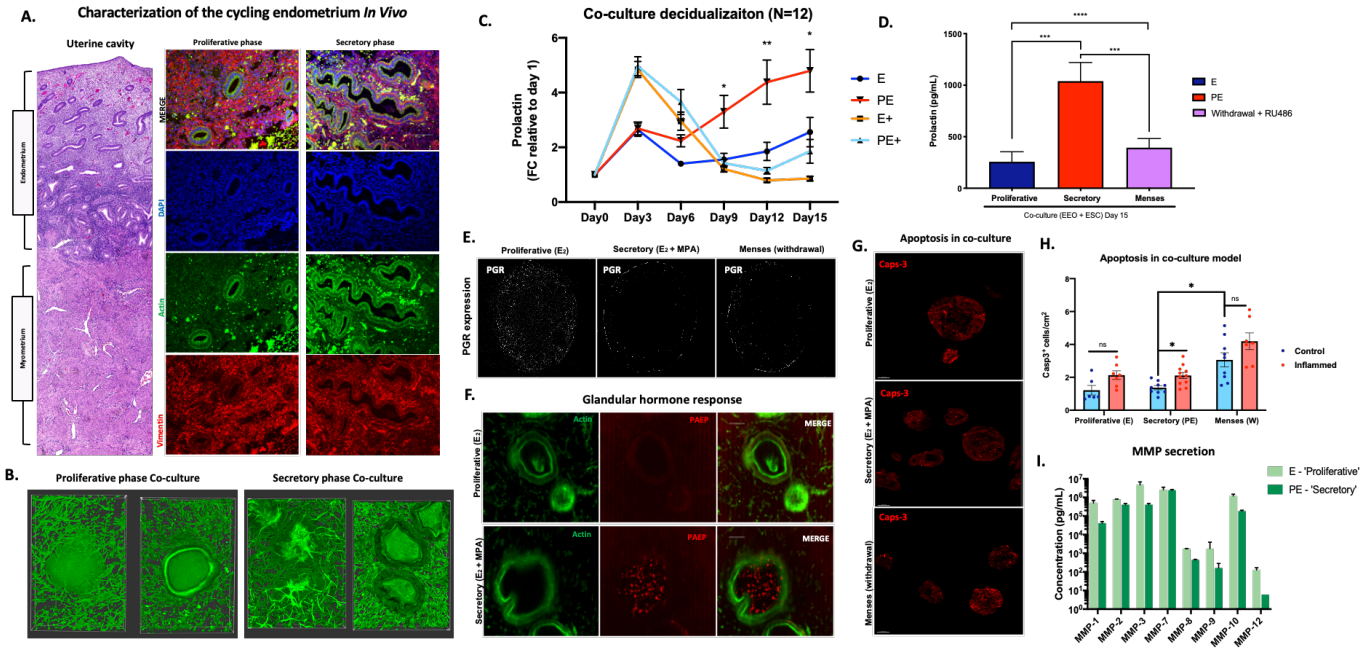

Figure 6. Functional analysis of inflammation in co-cultures in synthetic hydrogel reveals an endometriotic phenotype mediated by cell-cell communication.

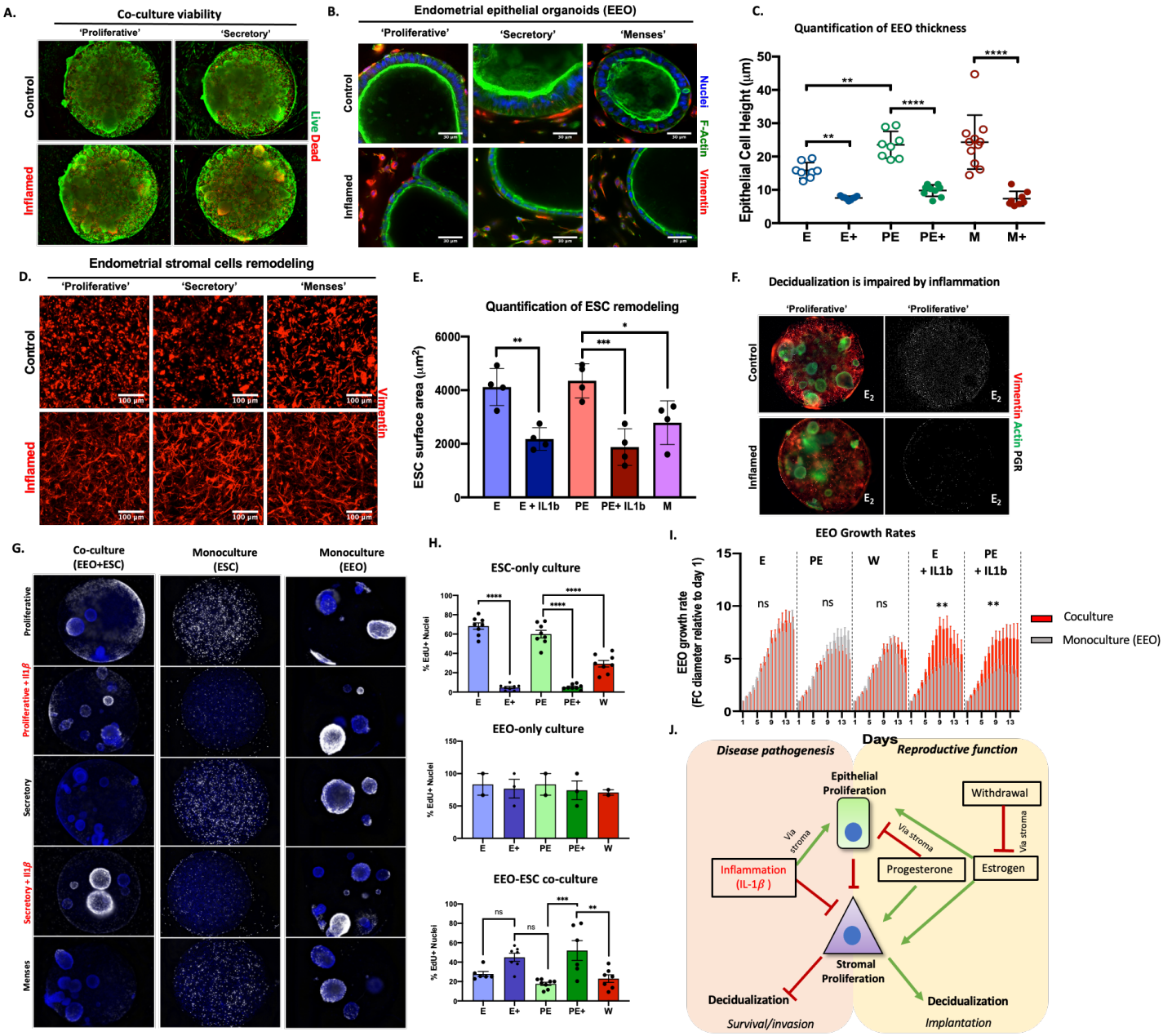

Supplementary Figures

Supplementary Fig 1. Characterization of the human endometrium using single cell transcriptomic analysis of the endometrium.

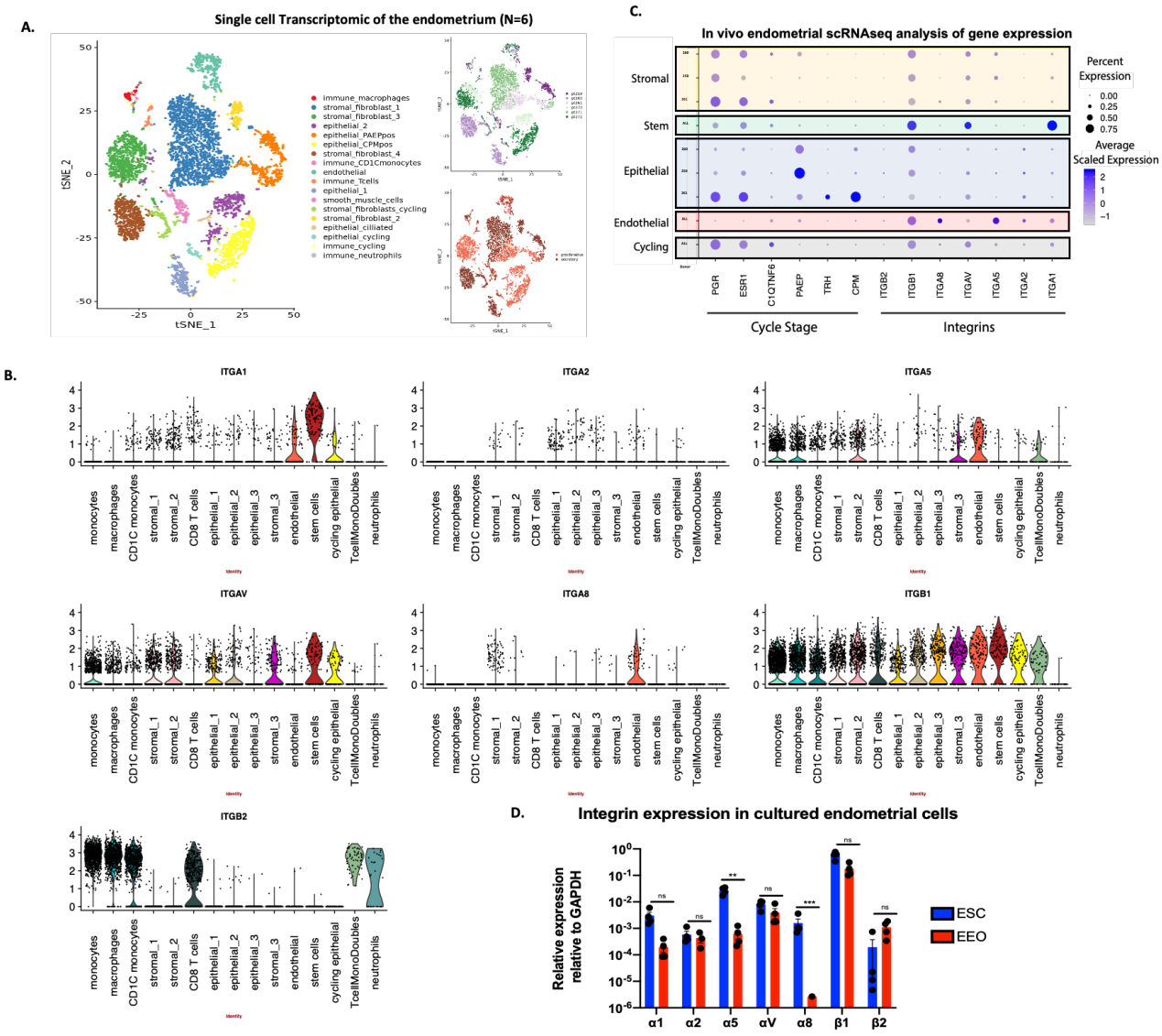

Supplementary Fig 2. Workflow for EEO generation, hydrogel generation and screening.

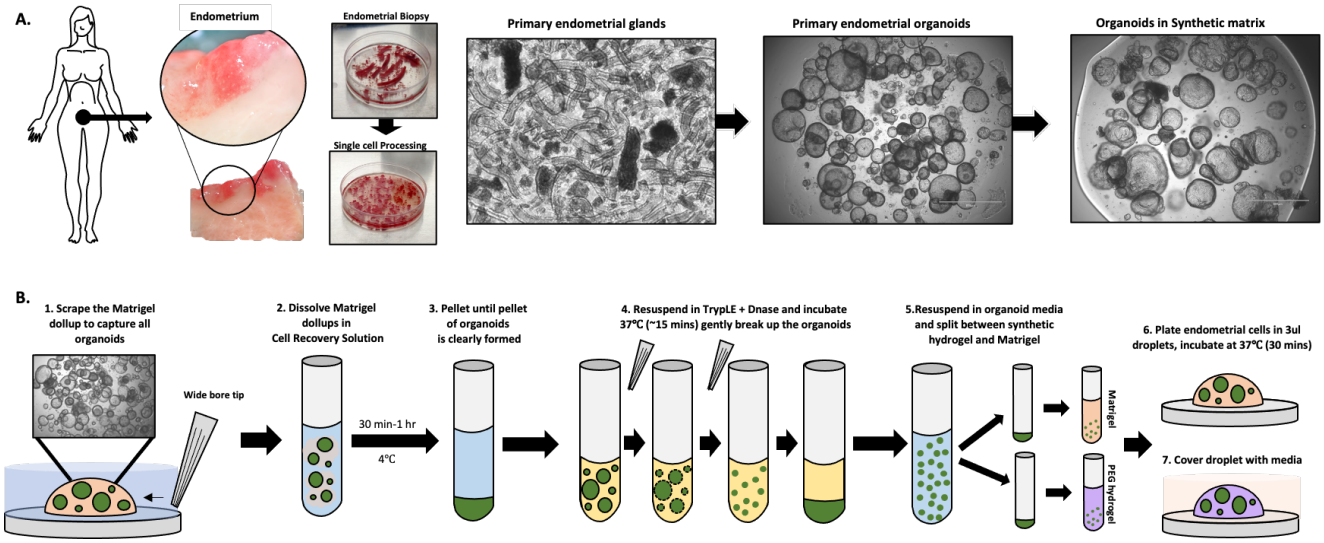

Supplementary Fig 3. Screening and quantification of EEO generation in synthetic matrices across donors.

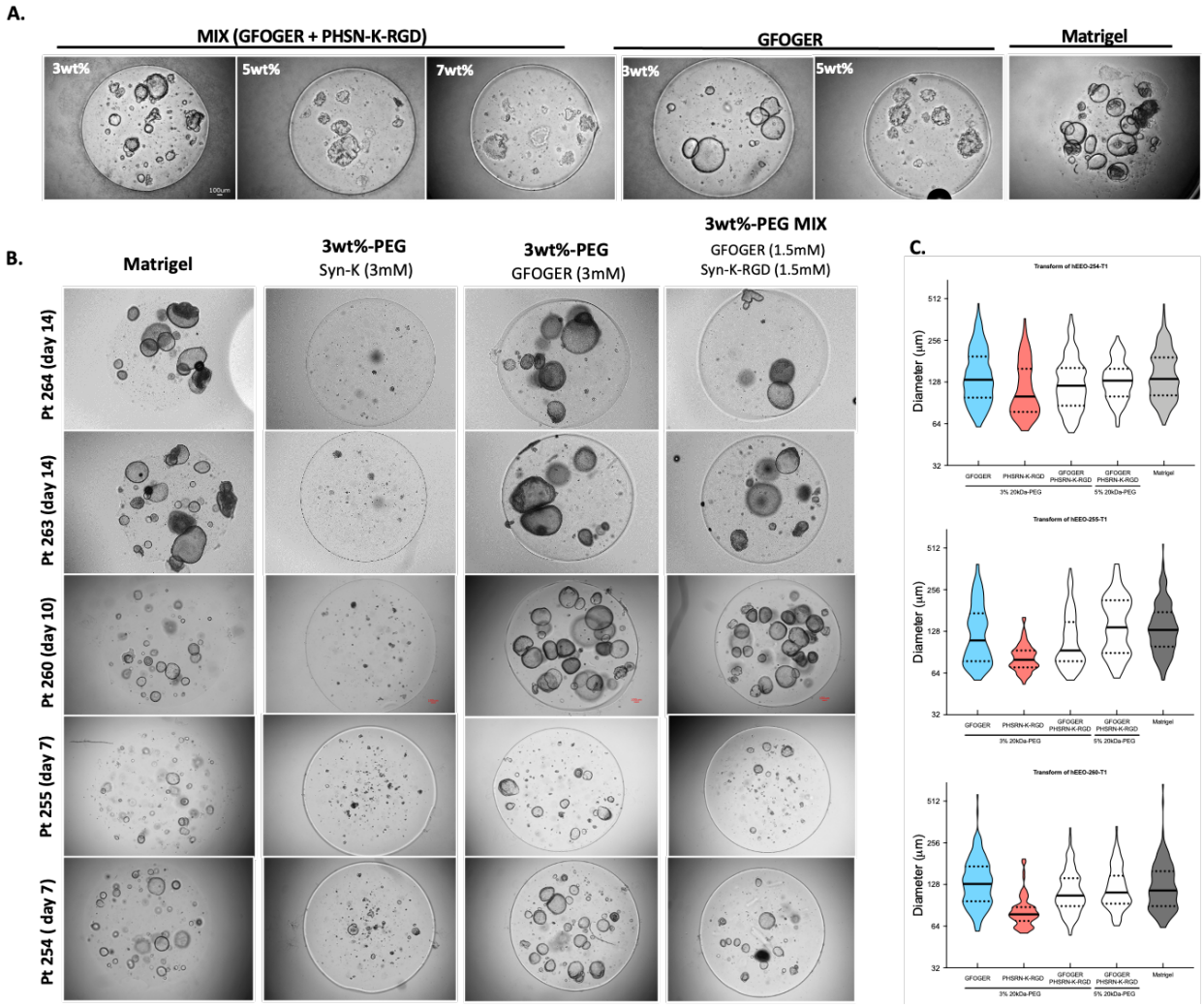

Supplementary Figure 4. Validation of EEOs cultured in PEG vs Matrigel.

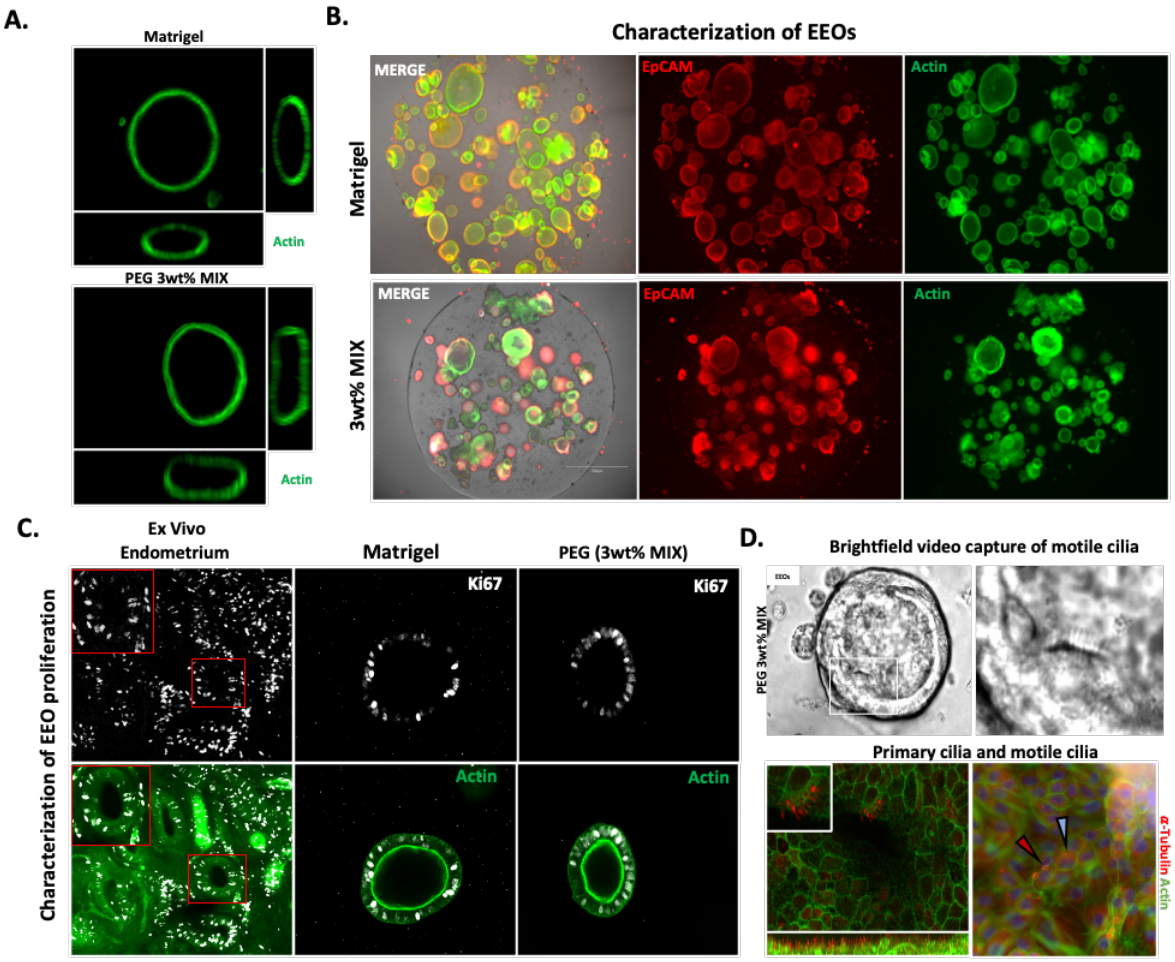

Supplementary Fig 5. Identifying cell ratios ex vivo for tissue modeling in vitro.

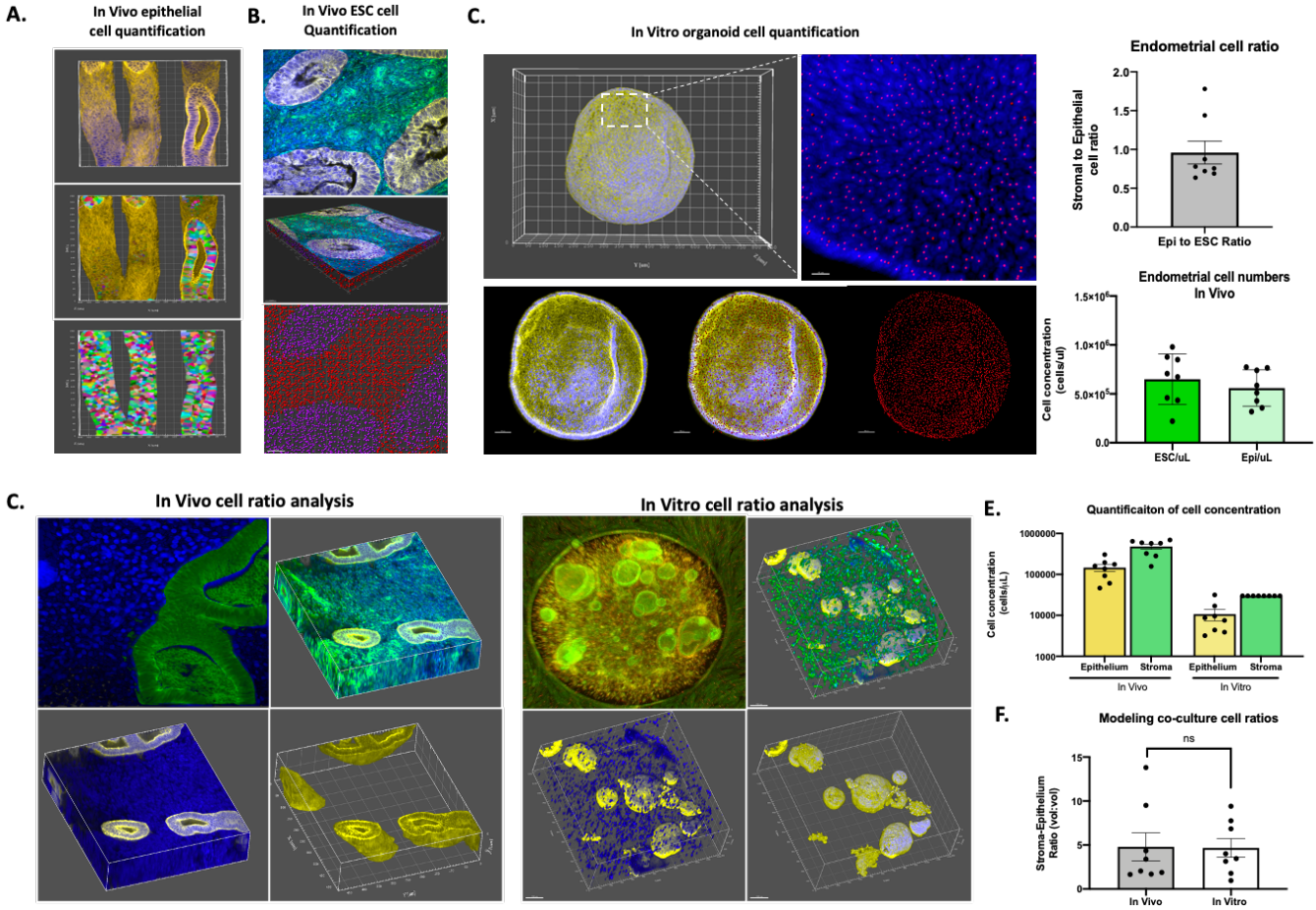

Supplementary Fig 6. Establishment and transcriptomic analysis of monocultures and co-cocultures.

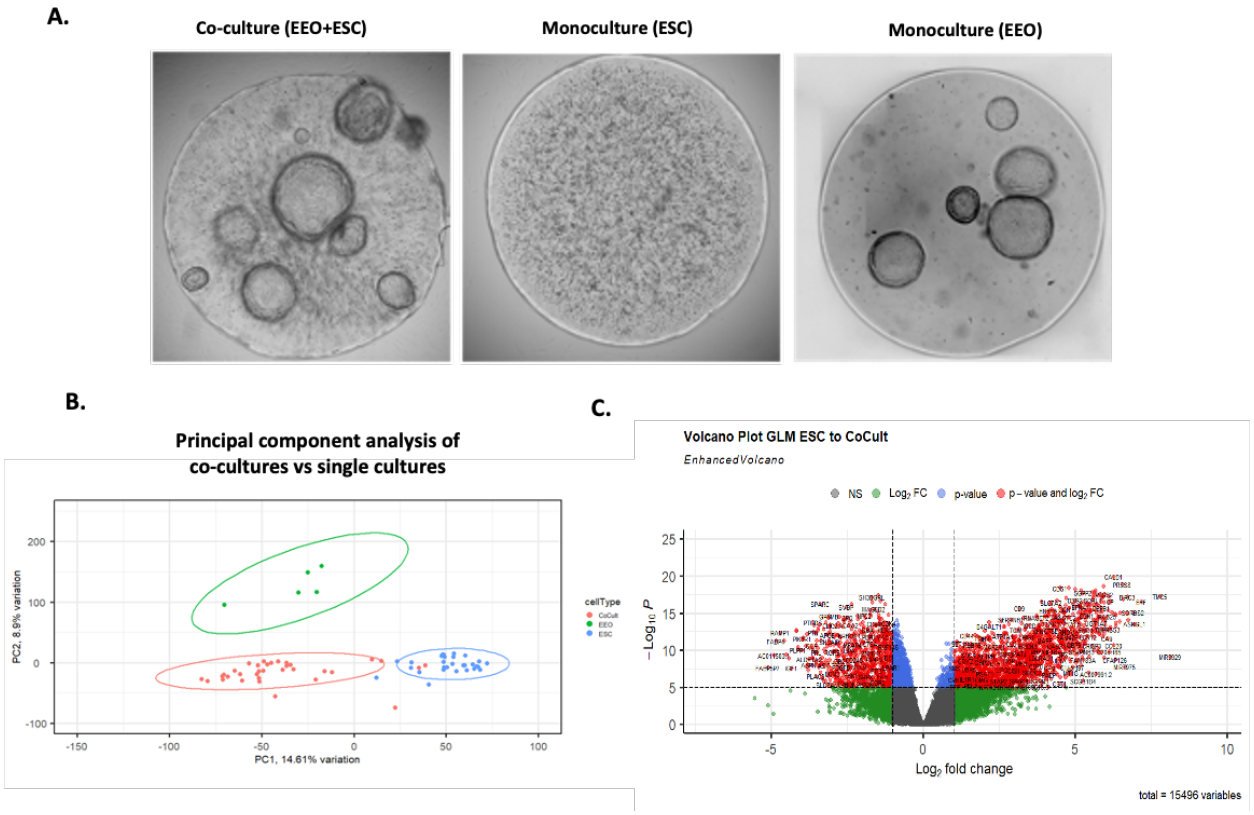

Supplementary Fig 3. Functional validation of endometrial-coculture recapitulation of the menstrual cycle in vitro.

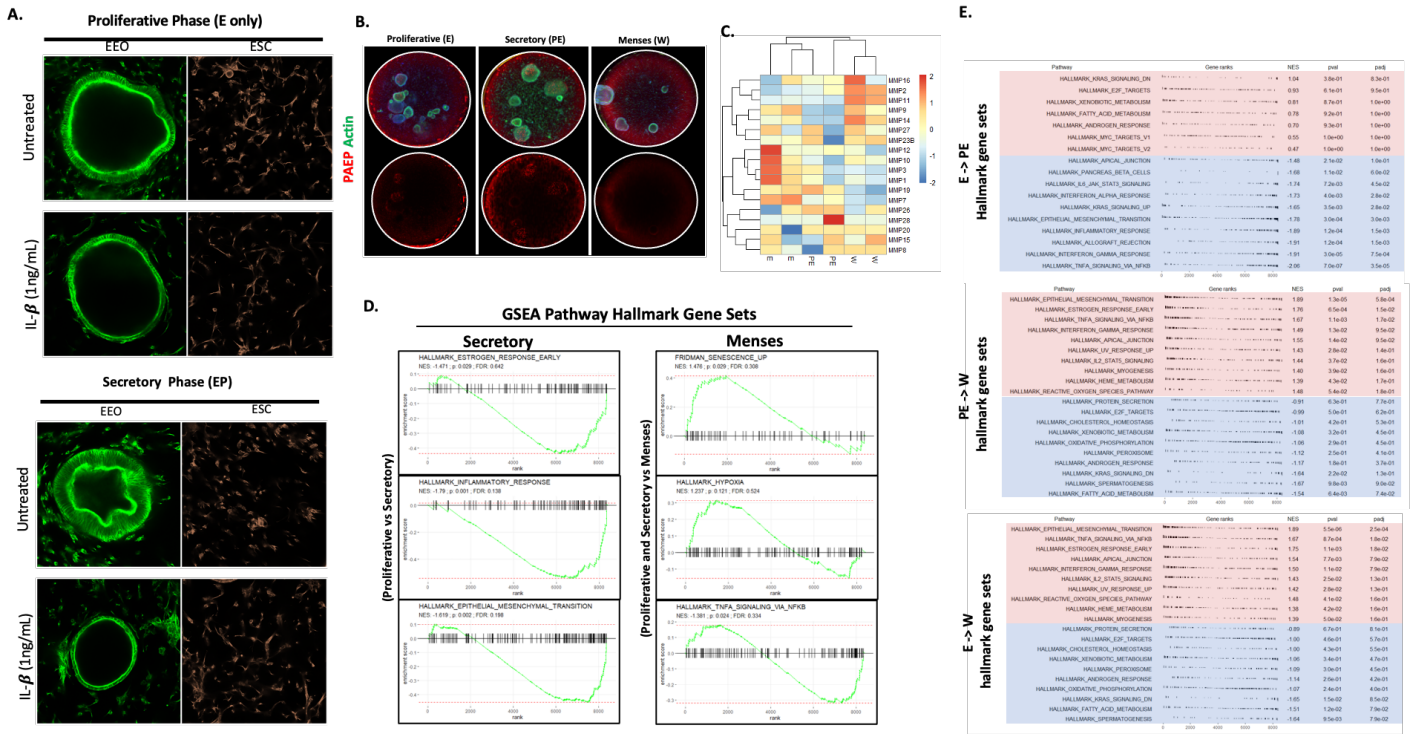

Supplementary Fig 4. Apoptosis is increased in the menstrual phase of the co-culture model and in the inflamed endometrium and corresponding viability is decreased in the inflamed group.

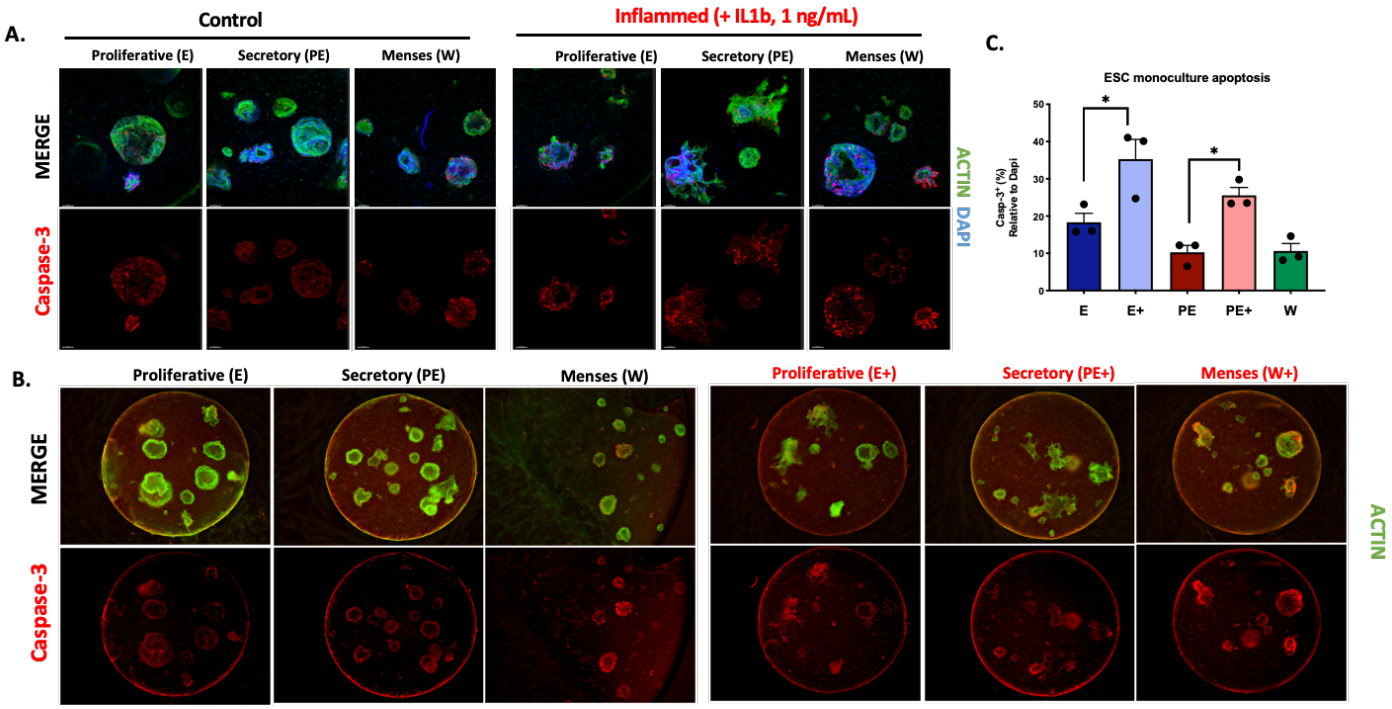

Supplementary Fig 9. Viability in the co-culture models at day 15.

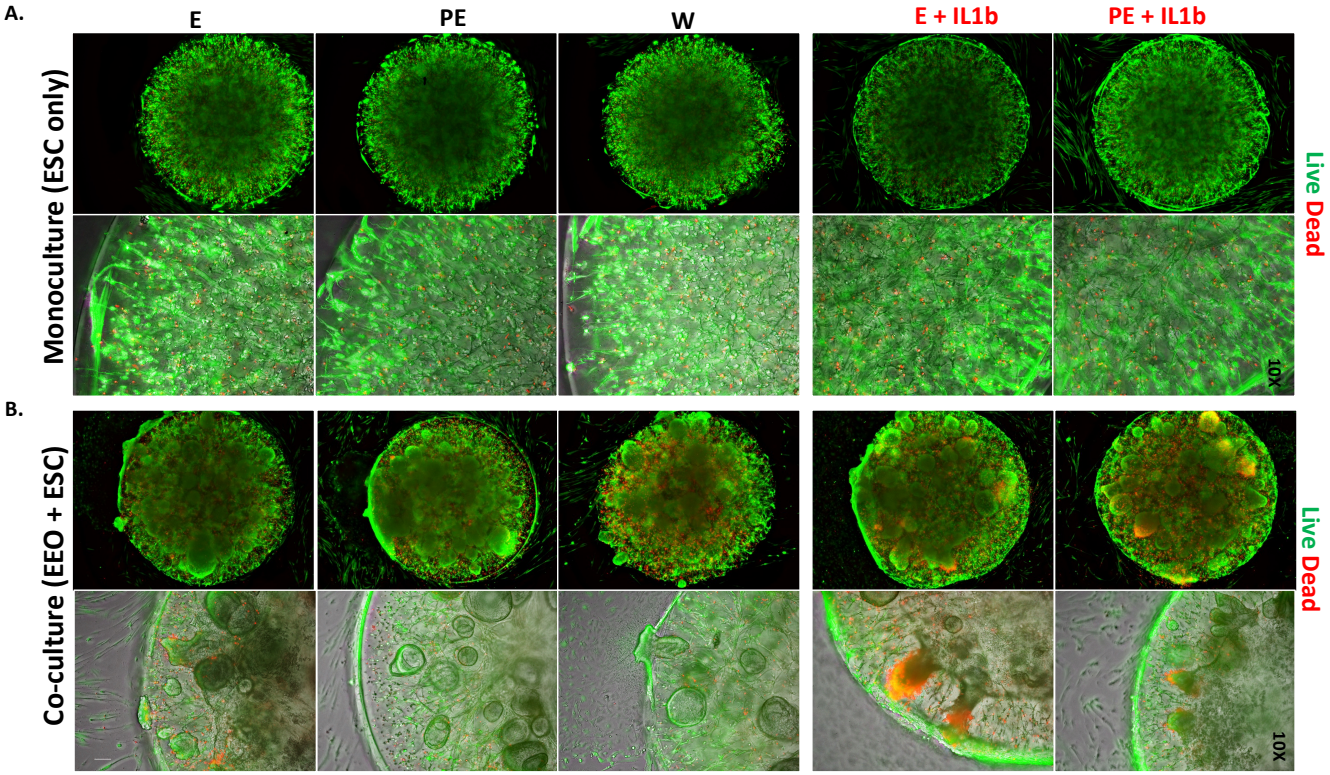

Supplementary Fig 10. Inflammation disrupts ESC remodeling and morphology.

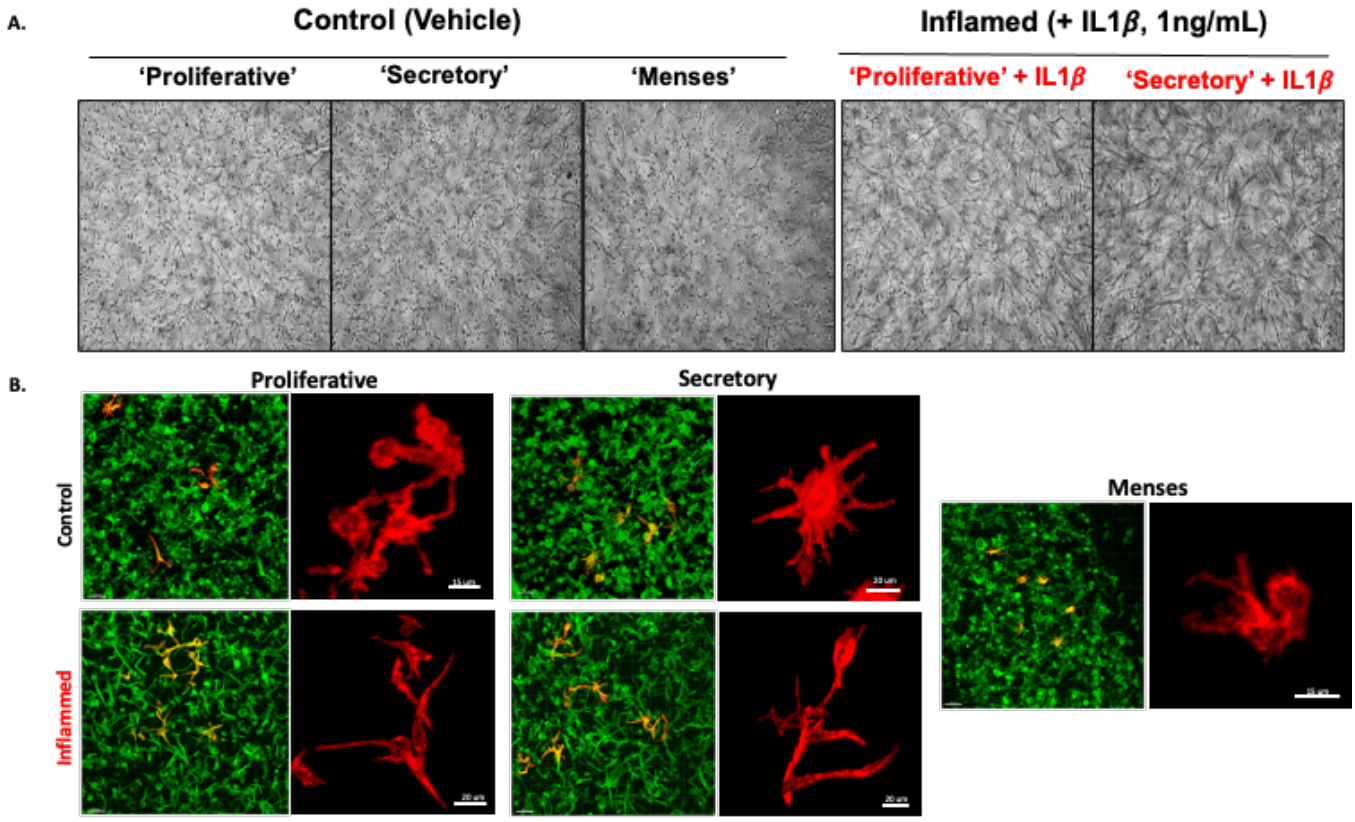

Supplementary Fig 11. Co-cultures treated with IL1β have transcriptomic profiles consistent with inflamed endometrial states.

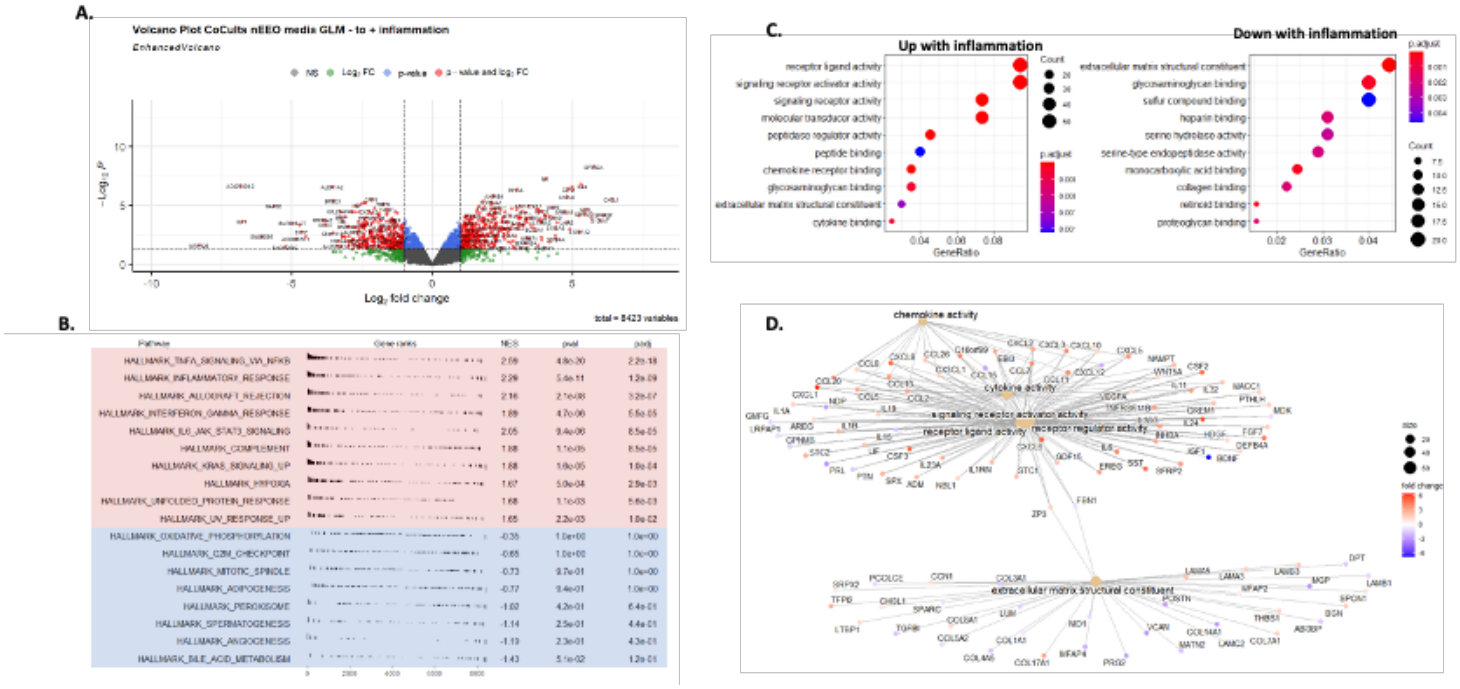

Supplementary Fig 12. Functional and molecular analysis of EEO growth rates.

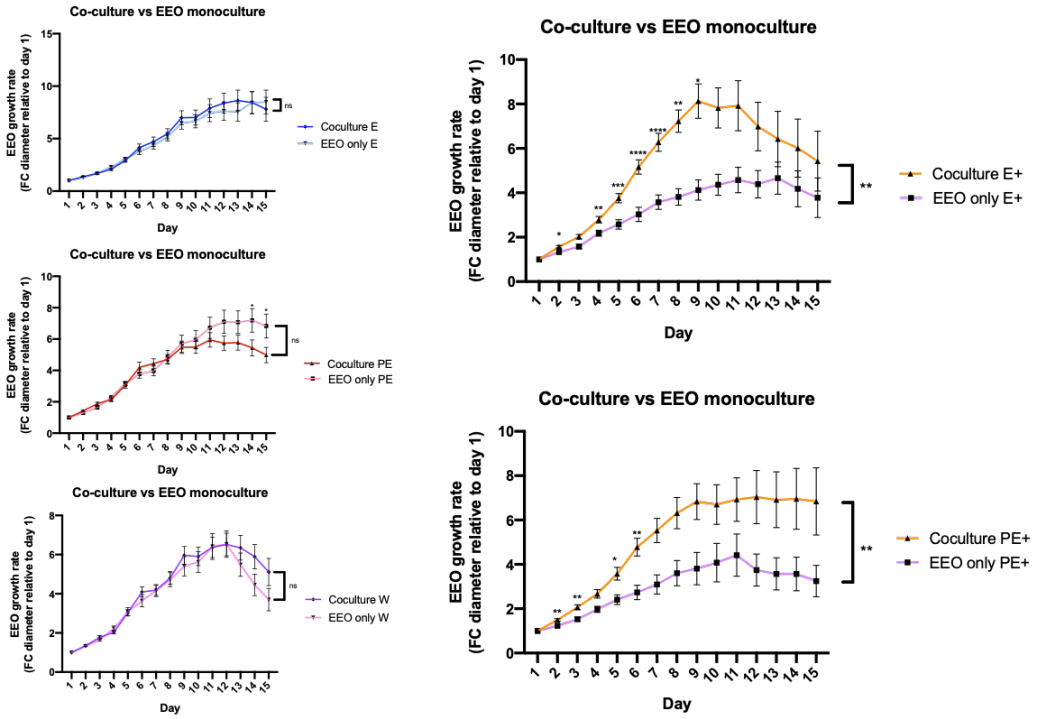

Supplementary Fig 13. Temporal validation of inflammatory response on co-cultures via functional and protein analysis.

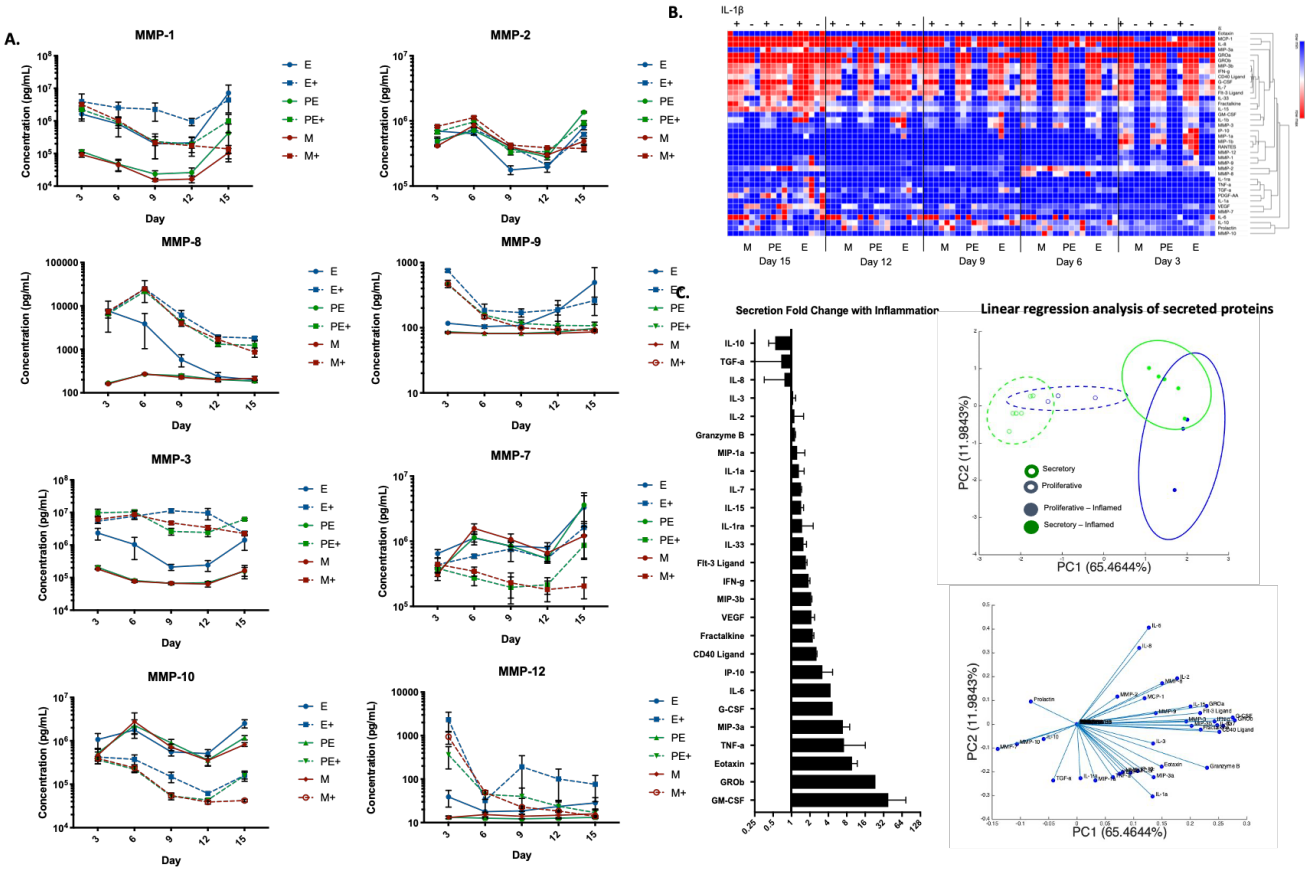

Supplementary Fig 14. EEOs can be generated and expanded directly into synthetic ECM from primary tissues.

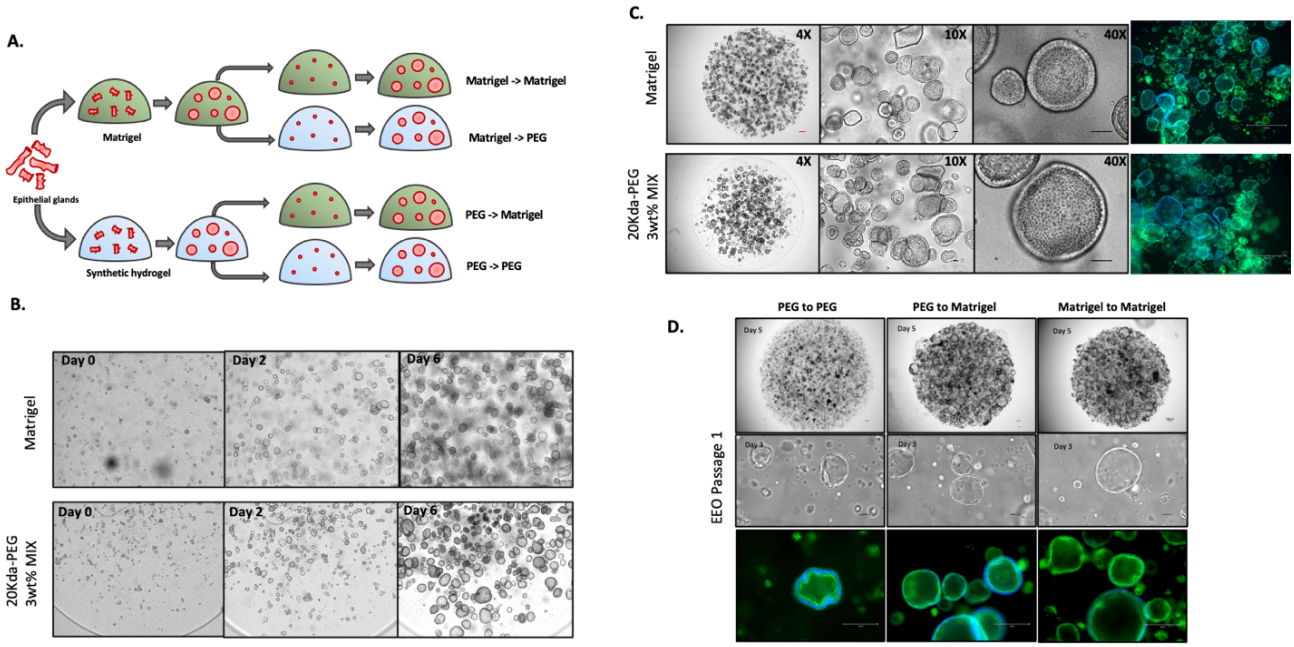

Supplementary Fig 15.

A.

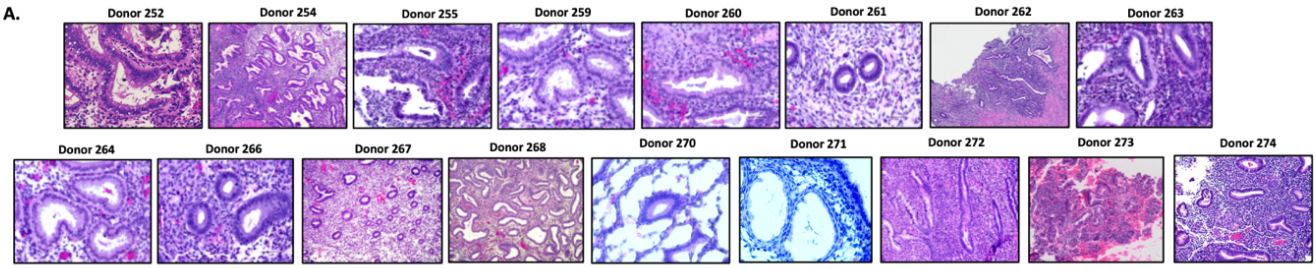

B.

Donor ID (Control/Osis)	DX Adenomyosis (Y)	DX Endometriosis (Y)	Other DX	Ex Vivo scRNAseq	Ex Vivo Proteimomics	Cell Separation	Co-culture Model	Co-culture bulk RNAseq	H&E (Y)	AGE	Cycle Phase	Gravity	Parity	Regular Cycles	Hormones in past 3 mo	NOTES
251	X		pelvic pain			X	X			42	Proliferative (CD13)			yes	no	
252			fibroid	X		X	X		X	39	Secretory			yes	no	
254		X				X			X	36	Secretory			yes	no	
255		X			X	X	X		X	40	Menses			yes	no	
259		X	Ov cyst	X		X	X	X	X	32	Secretory			yes	no	
260		X		X		X	X	X	X	27	Late secretory			yes	no	
261		X	Ovarian cyst	X		X			X	33	Proliferative			yes	no	
262			leiyoma						X	38	Proliferatve			yes	no	
263		X			X	X	X		X	40	Early Secretory	2	2	yes	no	weakly proliferated endometrium with focal stromal breakdown, squamous metaplasia of cervix,cyst, bloody, small biopsy
264			Leiyomata		X	X	X		X	43	Secretory	2	1	yes	no	Leiomyomata, big biopsy, good
266					X	X	X		X	30	Proliferative	4	4	yes	no	
267	X	X			X				X	43	Proliferative	2	2	yes	no	leiomyoma
268	X		leiomyomas		X	X	X		X	44	Secretory	2	1	yes	no	PF is bloody, multiple leiomyomas, chronic inflammation of the cervix
270			cyst adenoma	X	X	X	X	X	X	42	Early Secretory	1	0	yes	no	scRNA fresh and frozen, mucinous cystadenoma with focal dystrophic calcifications, corpus luteal cyst
271			leiomyoma	X	X	X	X	X	X	36	Secretory	3	2	yes	no	
272			AUB	X	X	X	X	X	X	42	Proliferative	2	2	no	no	PFC bloody
273	X	X			X	X			X	39	Late Secretory	2	2	yes	no	Late secretory
274	X	X			X				X	41	Proliferative	0	0	yes	no	

Videos

Motile cilia in synthetic PEG ECM (3wt% MIX)

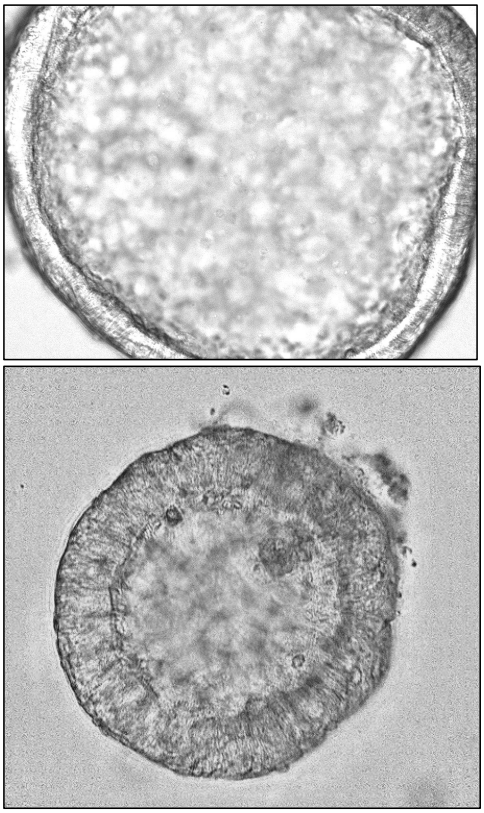

Motile cilia in vivo and in EEOs

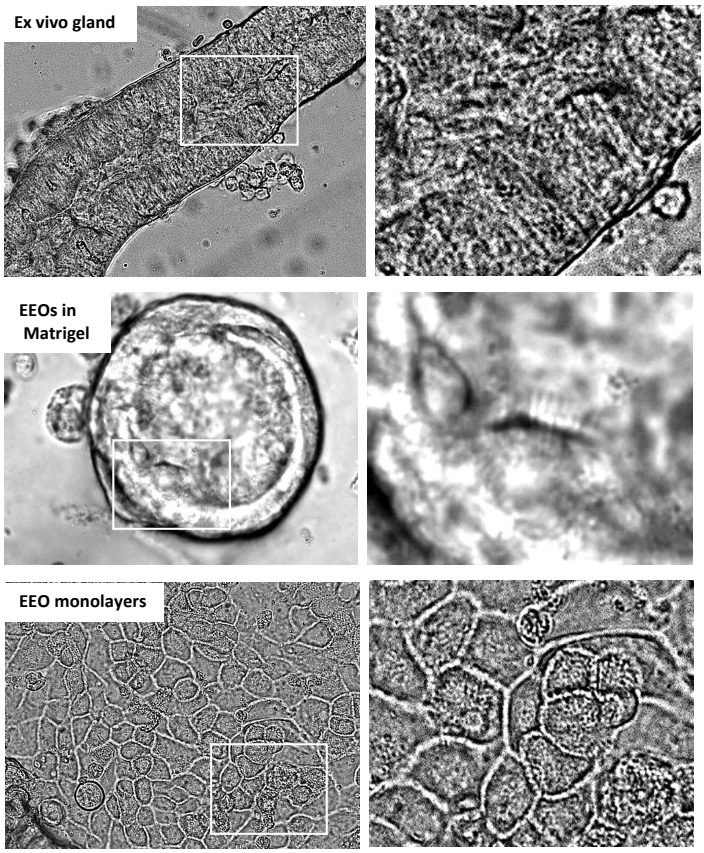

Video 1

Proliferative phase co-culture

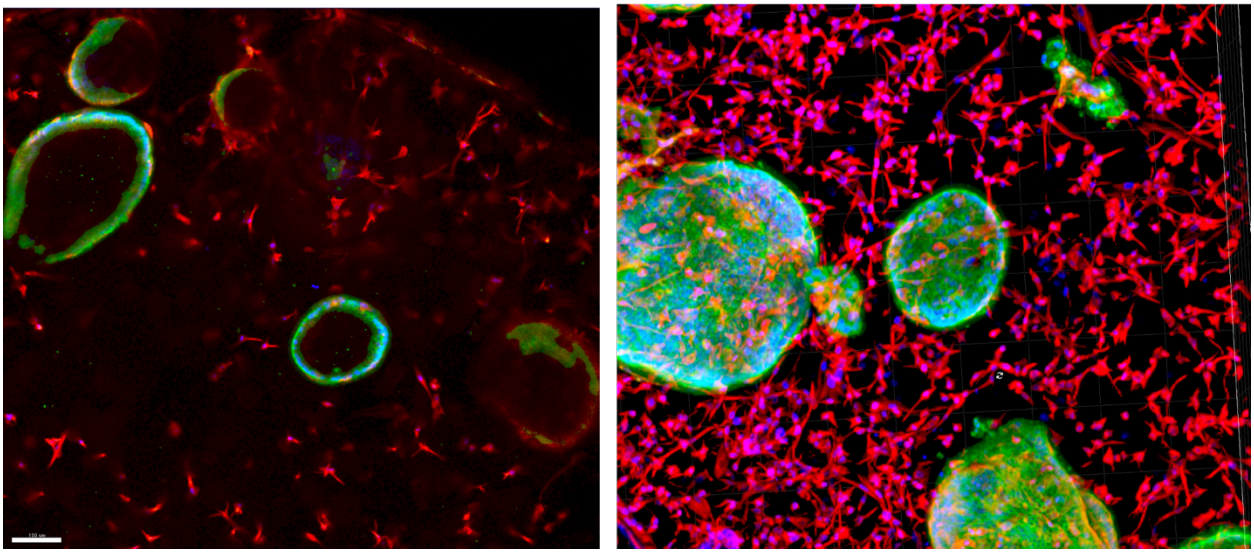

Video 2

Secretory phase co-culture

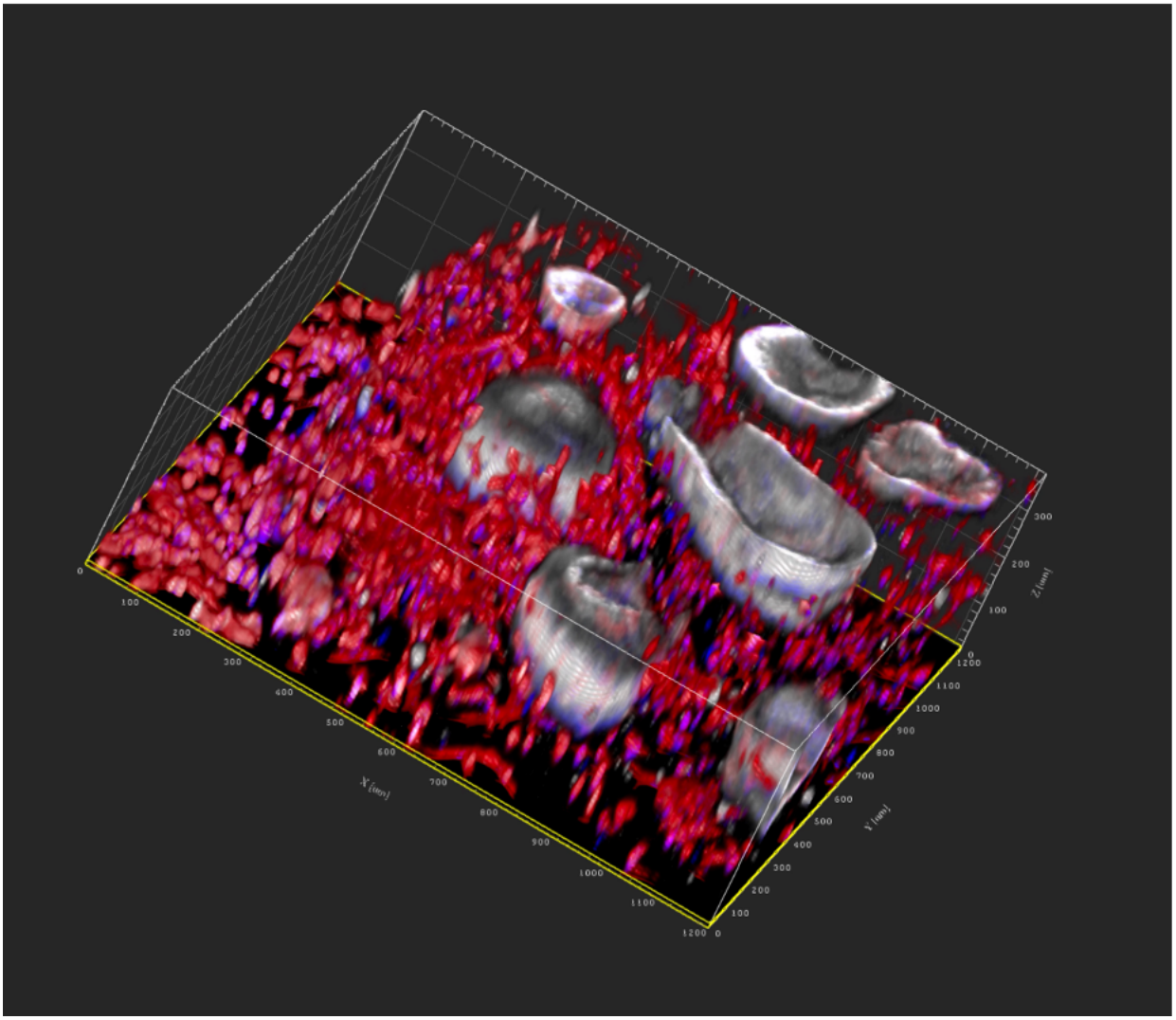

Video 3

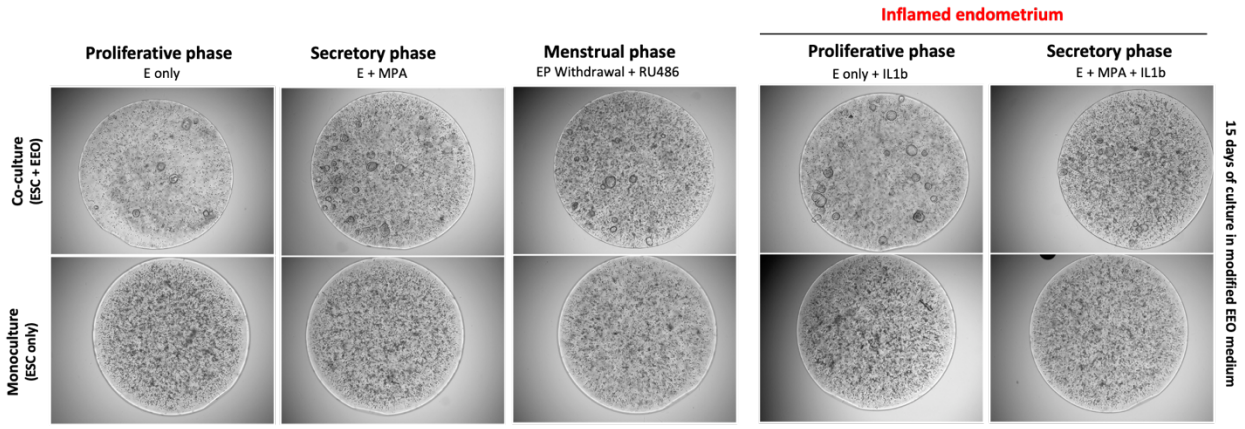
Inflamed endometrium
Proliferative phase
E only
Secretory phase
E + MPA
Menstrual phase
EP Withdrawal + RU486
Proliferative phase
E only + IL1b
Secretory phase
E + MPA + IL1b
Co-culture
(ESC + EEO)
Monoculture
(ESC only)
15 days of culture in modified EEO medium

Video 4

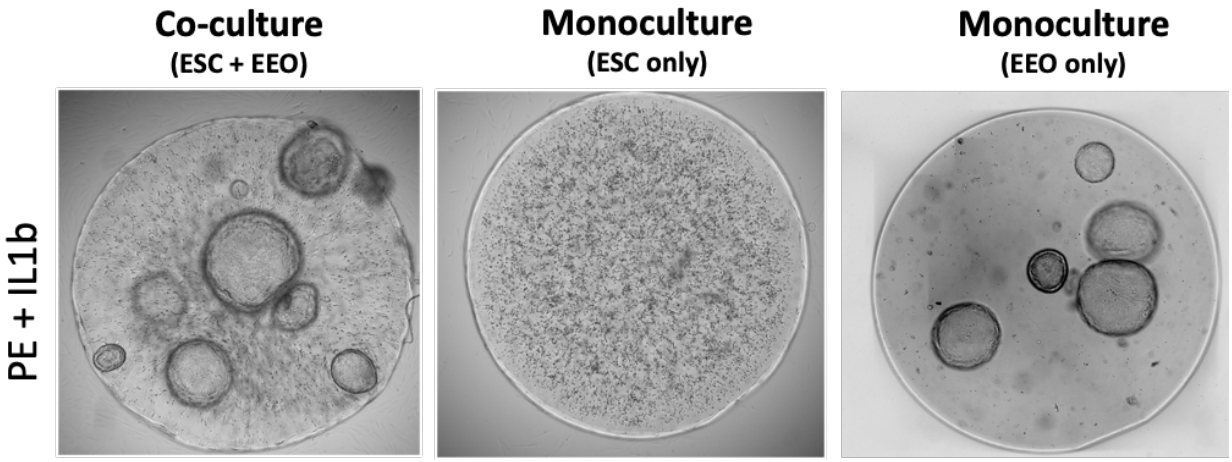
Co-culture
(ESC + EEO)
Monoculture
(ESC only)
Monoculture
(EEO only)
PE + IL1b

Video 5

1

2